J. Fluid Mech. (2012), *vol.* 708, *pp.* 539–575. © Cambridge University Press 2012
doi:10.1017/jfm.2012.332

Dynamic interaction of multiple buoyant jets

Adrian C. H. Lai[1] **and Joseph H. W. Lee**[2]†

[1] The Center for Environmental Sensing and Modelling, Singapore–MIT Alliance for Research and Technology Centre, 1 CREATE Way, CREATE Tower, Singapore 138602, Republic of Singapore

[2] Department of Civil and Environmental Engineering, The Hong Kong University of Science and Technology, Clear Water Bay, Hong Kong, People's Republic of China

(Received 18 January 2012; revised 17 June 2012; accepted 27 June 2012; first published online 10 August 2012)

An array of closely spaced round buoyant jets interact dynamically due to the pressure field induced by jet entrainment. Mutual jet attraction can result in a significant change in jet trajectories. Jet merging also leads to overlapping of the passive scalar fields associated with the individual jets, resulting in mixing characteristics that are drastically different from those of an independent free jet. A general semi-analytical model for the dynamic interaction of multiple buoyant jets in stagnant ambient conditions is proposed. The external irrotational flow field induced by the buoyant jets is computed by a distribution of point sinks with strength equal to the entrainment per unit length along the unknown jet trajectories and accounting for boundary effects. The buoyant jet trajectories are then determined by an iterative solution of an integral buoyant jet model by tracking the changes in the external entrainment flow and dynamic pressure fields. The velocity and concentration fields of the jet group are obtained by momentum or kinetic energy superposition for merged jets and plumes, respectively. The modelling approach is supported by numerical solution of the Reynolds-averaged Navier–Stokes equations. The model shows that jet merging and mixing can be significantly affected by jet interactions. Model predictions of the multiple jet trajectories, merging height, as well as the centreline velocity and concentration of the buoyant jet group are in good agreement with experimental data for: (i) a clustered momentum jet group; (ii) a turbulent plume pair; and (iii) a rosette buoyant jet group. Dynamic interactions between a jet group are shown to decrease with the addition of an ambient cross-flow.

Key words: jets, plumes/thermals, turbulent mixing

1. Introduction

The mixing of a round buoyant jet in an otherwise stagnant ambient fluid is well studied. For many problems in the natural and built environment, the buoyant jet flow is typically turbulent; ambient fluid from the surrounding environment is drawn into the jet through turbulent entrainment (Morton, Taylor & Turner 1956). This creates an irrotational flow external to the jet (Taylor 1958). The mean velocity and scalar concentration field across a free buoyant jet is approximately self-similar and Gaussian; predictions of the characteristic velocity and concentration along the unknown jet trajectory can be obtained by an integral jet model (e.g. Fischer *et al.*

† Email address for correspondence: jhwlee@ust.hk

https://doi.org/10.1017/jfm.2012.332 Published online by Cambridge University Press

1979; Turner 1986). In many problems, multiple buoyant jets are often discharged close to each other, with a variety of jet orientations and group configurations. For example, partially treated waste water from coastal cities is often discharged from a submarine ocean outfall in the form of multiple buoyant jets. The jet nozzles are typically arranged to maximize mixing with the ambient fluid; the buoyant jets are often discharged alternately from opposite sides of a diffuser, or as a rosette jet group clustered around the circumference of an outfall riser. Multiple air pollution sources induced by a heat island effect, as well as electronic equipment and humans in an office enclosure, can also be regarded as multiple jet or plume clusters (Baines & Keffer 1974; Linden 1999). Jet/plume interaction is also relevant to the design of cooling towers (Pera & Gebhart 1975) and the feeding pattern of bivalves (Monismith *et al.* 1990).

Multiple buoyant jets discharging in proximity interact dynamically due to the jet-induced flow and pressure field; the mixing of the jet group can be significantly affected by the interaction. The induced pressure field causes the jets to deflect towards each other and results in an altered jet trajectory that can be drastically different from that of a free jet. This tendency for jet mutual attraction has been observed in clustered jet groups (Baines & Keffer 1974), in alternating diffuser discharges whereby the jets discharge alternately in opposite directions from a diffuser pipe (Liseth 1970, 1976), in a turbulent plume pair (Kaye & Linden 2004) and in a rosette buoyant jet group (Seo, Kwon & Yeo 2004; Kwon 2005).

The interaction of dual plane momentum jets has been experimentally measured in an early study (Miller & Comings 1960). Pera & Gebhart (1975) studied the interaction of plane and axisymmetric convection plumes and developed an analytical model for the merging height of two-dimensional (2D) plumes. The pressure difference between the inner and outer sides of the cavity formed by two sides of the plume is obtained by assuming a uniform velocity profile in the cavity; the model is only applicable to 2D plumes. They also observed that the interaction of adjacent axisymmetric plumes is much less profound than that between 2D plumes. A similar model was developed for studying the merging height of twin plane jets (Marsters 1977). The 2D flow induced by multiple unidirectional momentum jets in shallow water was studied using an inviscid line momentum source model (Lee & Jirka 1980; Lee & Greenberg 1984).

A number of studies attempted to account for the interaction of an array of round buoyant jets. Based solely on kinematic considerations, Sorrell & Smith (1982) assumed that buoyant jets from the two sides of an alternating diffuser approach each other at a velocity proportional to the entrainment velocity; however, the proportionality constant was found to be substantially larger than can be justified on physical grounds. The pressure reduction in the cavity of merging jets from an alternating diffuser was also incorporated in an integral jet model (Davidson 1989); however, the model was able to predict the jet interaction only qualitatively.

All of the above theories deal with a simple symmetrical jet group configuration; the model predictions are also somewhat sensitive to the control volume definitions in the integral model formulation. More recently, the kinematic interaction of a turbulent plume pair has been studied (Kaye & Linden 2004); the plumes are assumed to be advected towards each other by the induced entrainment velocity computed by a potential flow theory. Whereas the predictions are in reasonable agreement with data for plumes of equal strength, the merging heights for plumes of unequal buoyancy flux are substantially over-predicted. The predictions are sensitive to the choice of the entrainment coefficient, and it is difficult to generalize the model (e.g. sources at different levels). Numerical computational fluid dynamics (CFD) studies of alternating

https://doi.org/10.1017/jfm.2012.332 Published online by Cambridge University Press

diffuser jets have also been attempted (Kuang *et al.* 2006). The merging process of neighbouring jets from initially a three-dimensional (3D) to eventually a 2D jet was also revealed. A negative pressure cavity was found between the two curtains of jets on each side of the diffuser.

In addition to the jet trajectory, the velocity and scalar concentration fields of a merged jet group are also of interest. At a certain distance from the source, the jets will eventually merge with each other to form a single rising buoyant jet. The representation of the merged jet group by an equivalent single jet/plume appears to be successful far from the source for some problems (Baines & Keffer 1974; Kaye & Linden 2004). Nevertheless, experiments with rosette jet groups (Roberts & Snyder 1993*b*) showed that in general the merged jet group characteristics are dependent on the 3D jet group configuration even for the same total buoyancy flux of the jet group.

Despite the many previous studies on multiple jet interaction, a general theory to account for the interaction of multiple buoyant jets with arbitrary configuration is hitherto unavailable. In this paper, a general semi-analytical model for the dynamic interaction of multiple buoyant jets is proposed. The jet-induced external flow field is computed using a 3D potential flow model by treating each individual jet independently as a series of point sinks of known strength based on free jet theory. The dynamic effect is incorporated into a jet integral model by tracking the changes in the external entrainment flow and pressure fields, and solving for the 3D trajectory of each individual jet using an iterative scheme. The velocity and tracer concentration fields of the jet group subsequent to jet merging are computed using momentum or kinetic energy superposition for jets and plumes, respectively. The validity of the modelling approach is demonstrated by comparison with CFD model computations. Model predictions are compared with experimental data for: (i) a clustered momentum jet group; (ii) a turbulent plume pair; and (iii) a rosette buoyant jet group.

2. A general theory for the dynamic interaction of buoyant jets

Consider a group of multiple buoyant jets, each with nozzle diameter D, initial velocity u_o, concentration c_o, source fluid density ρ_o, discharging into an otherwise stagnant ambient with uniform density ρ_a and depth H (figure 1*a*). Each jet discharges at an inclined vertical angle ϕ_o with respect to the horizontal plane and horizontal angle θ_o with respect to the x axis. Each buoyant jet is characterized by an initial specific volume flux $Q_o = (\pi D^2/4)u_o$, specific kinematic momentum flux $M_o = Q_o u_o$ and specific buoyancy flux $F_o = Q_o g'_o$, where g is the acceleration due to gravity and $g'_o = (\Delta\rho_o/\rho_a)g = ((\rho_a - \rho_o)/\rho_a)g$ is the reduced gravity. Each individual jet behaves initially like an independent free jet, entraining the surrounding fluid and inducing an irrotational flow field. The reduced pressure in the confined space between adjacent jets tends to draw the jets together, resulting in jet trajectories that are drastically different from those of free jets. The altered jet trajectories then induce a new external flow and pressure field that further influence the jet group, and this feedback mechanism continues until the steady state is reached. The proposed model mimics this physical process by accounting for the jet-induced external flow and its feedback to the individual jets using an iterative scheme.

2.1. *Flow and pressure field induced by a buoyant jet group in stagnant ambient fluid*

The jet-induced external irrotational flow field can be modelled by a line sink with prescribed strength (Taylor 1958; Kaye & Linden 2004). In our model, the 3D external flow field induced by a general buoyant jet group is computed using a distribution of point sinks along the jet trajectory of each individual jet.

https://doi.org/10.1017/jfm.2012.332 Published online by Cambridge University Press

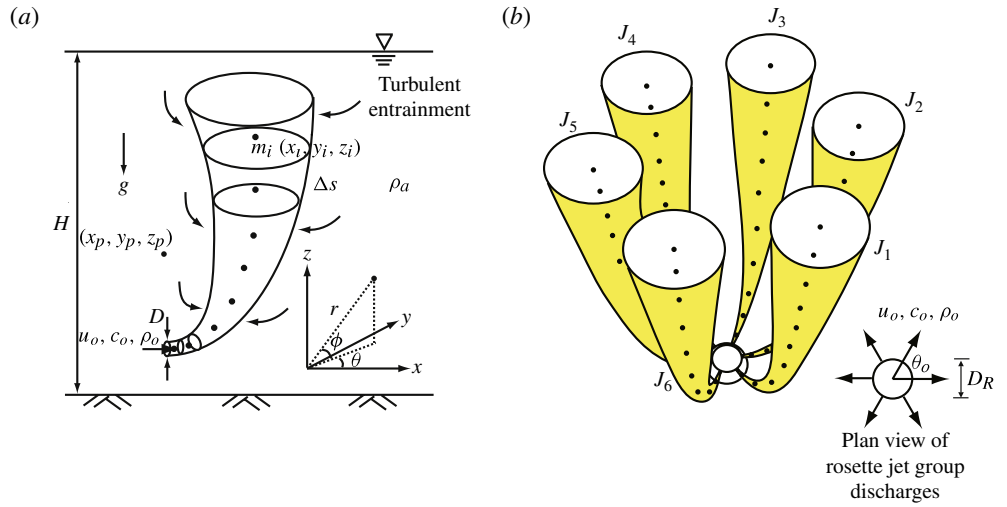


FIGURE 1. (Colour online) Sketch of (*a*) an inclined buoyant jet and (*b*) a rosette buoyant jet group ($N_J = 6$).

The buoyant jet is considered as a series of jet elements each with thickness Δs (figure 1*a*). Each jet element can be represented by a 3D point sink with strength $m_i = -\mathrm{d}Q/\mathrm{d}s$ at position $\boldsymbol{r_i} = (x_i, y_i, z_i)$. The velocity potential of this jet element is

$$\phi_i = \frac{m_i}{4\pi|\boldsymbol{r} - \boldsymbol{r_i}|}\Delta s, \tag{2.1}$$

where $\boldsymbol{r} = (x, y, z)$. The position and sink strength of each jet element can be obtained by an integral jet model (see later discussion). The induced radial velocity at an arbitrary point $\boldsymbol{r}$ due to the point sink at $\boldsymbol{r_i}$ is given by the negative gradient of the velocity potential (Lamb 1932; Milne-Thomson 1968):

$$u_r = -\frac{\partial \phi_i}{\partial r} = \frac{m_i}{4\pi\,|\boldsymbol{r} - \boldsymbol{r_i}|^2}\Delta s, \tag{2.2}$$

where $|\boldsymbol{r} - \boldsymbol{r_i}|^2 = (x - x_i)^2 + (y - y_i)^2 + (z - z_i)^2$. The induced velocity component in the x, y and z directions can be similarly found.

For multiple buoyant jet discharges (figure 1*b*), the N_J jets comprise N point sinks each. For a given point $\boldsymbol{r_p} = (x_p, y_p, z_p)$, the induced velocity due to each point sink is given by

$$(u_x)_{ij} = \frac{m_{ij}}{4\pi}\frac{(x_p - x_{ij})}{|\boldsymbol{r_p} - \boldsymbol{r_{ij}}|^3}\Delta s, \quad (u_y)_{ij} = \frac{m_{ij}}{4\pi}\frac{(y_p - y_{ij})}{|\boldsymbol{r_p} - \boldsymbol{r_{ij}}|^3}\Delta s, \quad (u_z)_{ij} = \frac{m_{ij}}{4\pi}\frac{(z_p - z_{ij})}{|\boldsymbol{r_p} - \boldsymbol{r_{ij}}|^3}\Delta s, \tag{2.3}$$

where $i = 1, \ldots, N$ and $j = 1, \ldots, N_J$. The external flow field induced by the jets is the superposition of all the external flows induced by the individual point sinks and is therefore given by

$$u_x = \sum_{j=1}^{N_J}\sum_{i=1}^{N}(u_x)_{ij}, \quad u_y = \sum_{j=1}^{N_J}\sum_{i=1}^{N}(u_y)_{ij}, \quad u_z = \sum_{j=1}^{N_J}\sum_{i=1}^{N}(u_z)_{ij}\,. \tag{2.4}$$

For the irrotational flow $\boldsymbol{q} = (q_x, q_y, q_z)$ outside of the jet(s), the pressure is related to the velocity by Bernoulli's equation $p_o - p = \rho(|\boldsymbol{q}|^2 - |\boldsymbol{q_o}|^2)/2$, where $|\boldsymbol{q}|^2 = u_x^2 + u_y^2 + u_z^2$ for the multiple jet-induced flow and $|\boldsymbol{q_o}|$ and p_o are reference

https://doi.org/10.1017/jfm.2012.332 Published online by Cambridge University Press

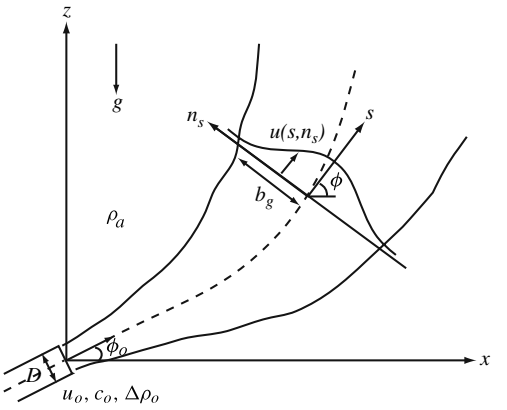


FIGURE 2. An inclined buoyant jet with self-similar Gaussian velocity profile assumption.

velocity magnitude and pressure taken at infinity (assumed to be zero without loss of generality). Thus we have

$$p = -\tfrac{1}{2}\rho\,|\boldsymbol{q}|^2\,. \tag{2.5}$$

The presence of solid boundaries is treated by the method of images (for stratified ambient density, the maximum rise height of the jet is regarded as the 'boundary'). In the applications considered herein, the domain of interest is large compared to the potential core length ($\approx 4D$–$6D$), which is neglected.

2.2. *Integral jet model accounting for dynamic pressure*

Consider a buoyant jet as defined in figure 1(*a*). The boundary layer approximation of the governing equations for continuity, momentum, tracer mass and buoyancy can be written in a local natural coordinate system (s, n_s) (figure 2), where s is the streamwise coordinate along the jet centreline and n_s is the direction orthogonal to s (e.g. Fischer *et al.* 1979; Lee & Chu 2003). Based on experimental observations, the velocity $u(s, n_s)$, tracer concentration $c(s, n_s)$ and density deficiency $\Delta\rho = \rho_a - \rho(s, n_s)$ in a jet cross-section are self-similar and Gaussian in shape, i.e.

$$u(s,n_s) = u_c(s)\mathrm{e}^{-n_s^2/b_g^2}, \quad c(s,n_s) = c_c(s)\mathrm{e}^{-n_s^2/\lambda^2 b_g^2}, \quad \Delta\rho(s,n_s) = \Delta\rho_c(s)\mathrm{e}^{-n_s^2/\lambda^2 b_g^2}, \tag{2.6}$$

where u_c, c_c and $\Delta\rho_c$ are the centreline velocity, tracer concentration and density deficiency, respectively, and b_g is the characteristic jet half-width defined by the location at which $u(s, n_s) = \mathrm{e}^{-1}u_c(s)$. Integrating the governing equations across the jet, we obtain the integral equations in terms of the jet volume flux $Q = \int u\,\mathrm{d}A = \int_0^\infty u(s, n_s)2\pi n_s\,\mathrm{d}n_s$, the specific momentum flux $M = \int u^2\,\mathrm{d}A$, the specific buoyancy flux $F = \int ug'\,\mathrm{d}A$ and the tracer mass flux $\Gamma = \int uc\,\mathrm{d}A$, i.e.

$$\frac{\mathrm{d}Q}{\mathrm{d}s} = 2\pi b_g(\alpha u_c), \tag{2.7}$$

$$\frac{\mathrm{d}M_z}{\mathrm{d}s} = \frac{\pi\lambda^2 b_g^2(\rho_a - \rho_c)g}{\rho_a}, \tag{2.8}$$

$$\frac{\mathrm{d}M_x}{\mathrm{d}s} = \frac{\mathrm{d}z}{\mathrm{d}s}\frac{\mathrm{d}M_x}{\mathrm{d}z} = -\sin\phi\left[\oint n_x\frac{p}{\rho}\,\mathrm{d}S_{cv} + \oint q_x(\boldsymbol{n}\cdot\boldsymbol{q})\,\mathrm{d}S_{cv}\right], \tag{2.9}$$

https://doi.org/10.1017/jfm.2012.332 Published online by Cambridge University Press

$$\frac{\mathrm{d}M_y}{\mathrm{d}s} = \frac{\mathrm{d}z}{\mathrm{d}s}\frac{\mathrm{d}M_y}{\mathrm{d}z} = -\sin\phi\left[\oint n_y \frac{p}{\rho}\,\mathrm{d}S_{cv} + \oint q_y(\boldsymbol{n}\cdot\boldsymbol{q})\,\mathrm{d}S_{cv}\right], \tag{2.10}$$

$$\frac{\mathrm{d}F}{\mathrm{d}s} = \frac{\pi u_c b_g^2}{\rho_a}\frac{\mathrm{d}\rho_a}{\mathrm{d}z}\sin\phi, \tag{2.11}$$

$$\frac{\mathrm{d}\Gamma}{\mathrm{d}s} = 0, \tag{2.12}$$

$$\frac{\mathrm{d}x}{\mathrm{d}s} = \cos\phi\cos\theta, \quad \frac{\mathrm{d}y}{\mathrm{d}s} = \cos\phi\sin\theta, \quad \frac{\mathrm{d}z}{\mathrm{d}s} = \sin\phi. \tag{2.13}$$

In the above governing equations, which can also be obtained by applying conservation principles to a local control volume normal to the jet axis, the Boussinesq approximation ($\Delta\rho/\rho \ll 1$) has been made. An entrainment hypothesis (Morton *et al.* 1956) is employed for turbulent closure (equation (2.7)); the turbulent entrainment is hypothesized to be driven by a characteristic local velocity (shear entrainment). The local entrainment velocity is assumed to be proportional to the centreline jet velocity, with α denoting the entrainment coefficient. Equation (2.8) shows that the vertical momentum is increased by the buoyancy forces. The horizontal momentum flux computed through the control volume balance of each jet element is incorporated into the x and y momentum equations in (2.9)–(2.10) (details in § 2.2.1). Dynamic effects are hence accounted for; the right-hand side of the equation is zero for a free jet (i.e. horizontal momentum flux is conserved). Equations (2.11) and (2.12) represent the conservation of jet buoyancy flux and tracer mass flux along the streamwise direction, respectively. The jet trajectory is given by (2.13).

The jet centreline variables u_c, c_c and ρ_c can be related to the integral fluxes via the Gaussian profile assumption as

$$Q = \pi u_c b_g^2, \quad M = \frac{\pi}{2}u_c^2 b_g^2, \quad F = \frac{\lambda^2}{1+\lambda^2}\pi u_c b_g^2\frac{(\rho_a-\rho_c)}{\rho_a}g, \quad \Gamma = \frac{\lambda^2}{1+\lambda^2}\pi u_c b_g^2 c_c. \tag{2.14}$$

The entrainment coefficient is determined as a function of the local jet densimetric Froude number $Fr_L = u_c/\sqrt{g(\Delta\rho_c/\rho_a)b_g}$ and the local vertical jet orientation ϕ: $\alpha = \alpha_j + (\alpha_p - \alpha_j)\,(Fr_p/Fr_L)^2\sin\phi$. The value of α varies from $\alpha_j = 0.057$ for a pure jet to $\alpha_p = 0.085$ for a pure plume. The ratio of concentration to velocity half-width is taken as $\lambda = 1.2$ (Fischer *et al.* 1979; Wood, Bell & Wilkinson 1993; Lee & Chu 2003), and Fr_p is the asymptotic plume densimetric Froude number (see appendix C). Equations (2.7)–(2.13) can then be expressed and solved in terms of the jet fluxes using a fourth-order Runge–Kutta scheme with initial conditions $(Q_o, M_{zo}, M_{xo}, M_{yo}, F_o, \Gamma_o, x_o, y_o, z_o)$ at the source.

2.2.1. *Computation of pressure force in horizontal momentum balance*

The dynamic effect on a jet can be accounted for by a momentum balance on each jet element with the multiple jet-induced flow and pressure field. Consider a control volume with arbitrary shape containing a jet element (figure 3); the pressure force is acting normal to the control surface, and flow enters or exits in an arbitrary direction. An exact momentum balance on the control volume in the xy plane gives (Milne-Thomson 1968):

$$\int_S \boldsymbol{n}\frac{p}{\rho}\,\mathrm{d}S = -\int_S \boldsymbol{q}(\boldsymbol{n}\cdot\boldsymbol{q})\,\mathrm{d}S, \tag{2.15}$$

https://doi.org/10.1017/jfm.2012.332 Published online by Cambridge University Press

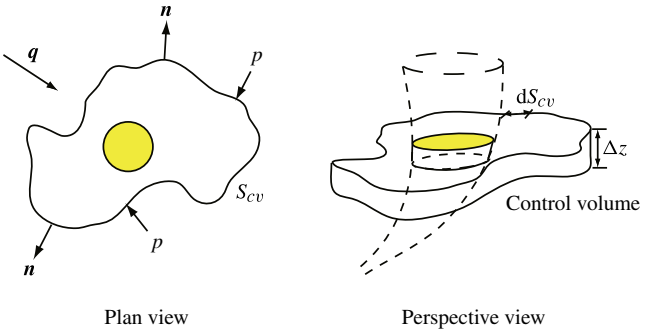


FIGURE 3. (Colour online) A control volume containing the jet element for horizontal momentum balance.

where S is the control surface and $\boldsymbol{n} = (n_x, n_y)$ is the normal vector to S (outward positive). The vertical change (along the z direction) of horizontal jet momentum in the xy plane can be expressed as

$$\Delta \boldsymbol{M}_{xy} = -\left[\oint \boldsymbol{n}\frac{p}{\rho}\,\mathrm{d}S_{cv} + \oint \boldsymbol{q}(\boldsymbol{n}\cdot\boldsymbol{q})\,\mathrm{d}S_{cv}\right]\Delta z, \tag{2.16}$$

where S_{cv} is the bounding curve of the control volume in the xy plane. In (2.9) and (2.10) the change in horizontal jet momentum flux in natural coordinates is determined via a momentum balance in Cartesian coordinates (figure 2). The orientation of the control volume chosen for the pressure computation is parallel to the xy plane. In the numerical implementation, the curve S_{cv} is discretized into a finite number of segments; the local normal vector $\boldsymbol{n}$ to every segment can be found through the segment coordinates. The changes in the horizontal jet momentum flux (in the x and y directions) through a distance of Δz are computed by summing up the effect on each segment. A detailed computation example is given in Lai (2009). The factor $\sin\phi$ in (2.9) and (2.10) is used to convert the computed momentum flux changes in Cartesian coordinates into natural coordinates as in the governing equations.

2.2.2. *Iterative solution of buoyant jet trajectory*

An iterative scheme is adopted to compute the buoyant jet characteristics with the dynamic effect incorporated (figure 4). Starting from a zero pressure condition (free buoyant jet), the governing equations for each individual jet are solved independently to give an initial set of free buoyant jet trajectories. Equations (2.3)–(2.5) are used to give the external flow and pressure field corresponding to the jet group. The set of parabolic governing equations (2.7)–(2.13), including the lateral momentum balance, are solved to obtain the revised trajectory, velocity and concentration of each individual buoyant jet. The external flow and pressure field of the jet group can then be updated, based on which a revised set of buoyant jet trajectories are solved. This iterative procedure continues until the jet trajectory solution converges. The dynamic interaction between two jets is assumed to exist until the outer edges of two adjacent jets intersect. Subsequent to this, the net horizontal momentum flux change of the composite jet is assumed to be zero and the jet trajectory is assumed to be vertical. This 'outer edge' is defined at b_g from the jet centreline throughout this paper unless otherwise specified. Convergence is declared when $\Delta x < 0.01\Delta s$.

In solving the multiple jet trajectories iteratively, the horizontal momentum flux into the control volume in the xy plane needs to be computed. This can be facilitated

https://doi.org/10.1017/jfm.2012.332 Published online by Cambridge University Press

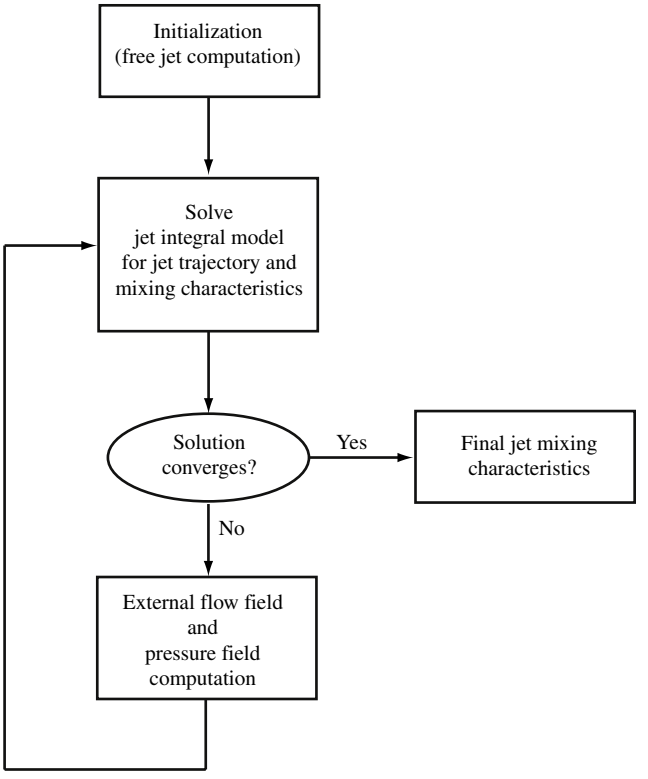


FIGURE 4. Semi-analytical model for dynamic interaction of buoyant jets.

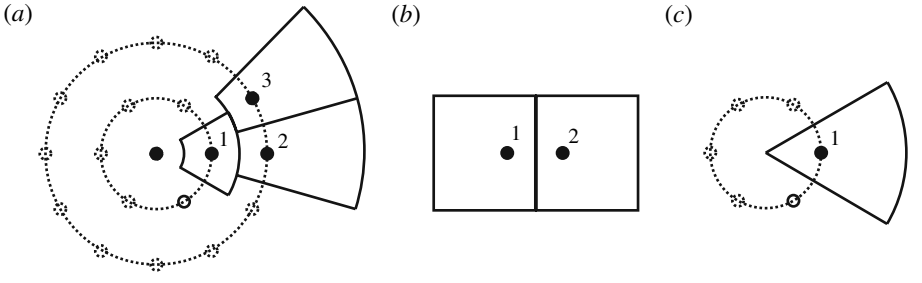


FIGURE 5. Control volumes choice for: (*a*) a clustered jet group; (*b*) an unequal turbulent plume pair; and (*c*) a six-jet rosette buoyant jet group.

by choosing the control surfaces at no-flux boundaries when they exist. The control volumes selected for several jet group configurations for the test problems (see later discussion) are illustrated in figure 5. The dynamic jet interaction is treated by solving the governing equations using three control volumes for a 19-jet clustered configuration (figure 5*a*), two control volumes for a plume pair with unequal buoyancy fluxes (figure 5*b*), and one control volume for a six-jet rosette jet group, with the control surfaces chosen at no-flux boundaries by symmetry (figure 5*c*).

The model predictions are not sensitive to the exact choice of an appropriately defined control volume (see example in appendix F), as the horizontal momentum

https://doi.org/10.1017/jfm.2012.332 Published online by Cambridge University Press

changes due to both the flow and pressure field have been accounted for. The above semi-analytical modelling framework is supported by extensive numerical experimentation using CFD models (see appendix A).

3. Superposition model for merged jets and plumes

The model for the dynamic interaction of buoyant jets accounts for the mutual attraction of jets in a jet group. The velocity field of multiple momentum jets after merging can be computed using the superposition technique based on Reichardt's hypothesis (Knystautas 1964). Based on the observation that the radial distribution of momentum flux in a round jet follows an error function distribution, Reichardt's inductive hypothesis for turbulent closure assumes that the lateral gradient of the shear stress is proportional to the transverse gradient of the x momentum (Hinze 1975) (for a pure jet discharging in the x direction). This results in a linear equation in terms of the jet momentum flux u^2. The linearity in jet momentum permits the method of superposition to be used in multiple jets; the local momentum flux can be considered as the net summation of the momentum flux contributions from all the individual axisymmetric jets (appendix B). The approach has been used successfully to study merging of a row of round jets into a quasi-2D jet (Knystautas 1964), and the prediction of the velocity field of multiple parallel turbulent jets in a stagnant ambient fluid (Pani & Dash 1983). The approach has also been extended to the study of multiple co-flow jets (Pani, Lai & Lee 2009). Key details of the method are given in appendix B for completeness.

Referring to figure 1, for a given vertical level $z = z_l$, the jet centreline position (x_i, y_i, z_l), centreline velocity $u_{ci}(x_i, y_i, z_l)$ and centreline concentration $c_{ci}(x_i, y_i, z_l)$ (and density deficiency $\Delta\rho$) of the ith deflected jet are computed by the dynamic jet model in § 2. To compute the jet group velocity field by the method of superposition, we assume the velocity distribution $u_i(x, y, z_l)$ of the ith deflected jet to be locally Gaussian relative to the jet centreline, i.e. $u_i(x, y, z_l) = u_{ci}(x_i, y_i, z_l)\mathrm{e}^{[(x-x_i)^2+(y-y_i)^2]/b_g(z_l)^2}$ (and similarly for the tracer concentration with half-width λb_g). The mean square velocity (momentum) of each jet at every point of interest $u_i(x, y, z_l)^2$ is then superimposed to give the momentum corresponding to the jet group $u_{N_J}(x, y, z_l)^2$ (figure 6). It follows that, if there are N_J jets each with velocity u_i in a jet group, its velocity u_{N_J} can be obtained by solving

$$u_{N_J} = \left(\sum_{i=1}^{N_J} u_i^2\right)^{1/2}. \tag{3.1}$$

The theory is valid for pure jet discharges. The superposition approach has recently been extended to pure plume discharges by Yannopoulos & Noutsopoulos (2006). They assumed that the kinetic energy of a merged plume can be obtained by superposition of the kinetic energy of each individual plume (see also appendix C):

$$u_{N_J} \approx \left(\sum_{i=1}^{N_J} u_i^3\right)^{1/3}. \tag{3.2}$$

As the advective diffusion equation for conservation of tracer mass is linear, Reichardt's hypothesis has also been extended to the lateral transport of tracer mass. It is shown that the concentration field of multiple circular turbulent jets can be obtained by superposition of the local time-mean mass flux $\overline{UC} \approx uc$ (Hodgson,

https://doi.org/10.1017/jfm.2012.332 Published online by Cambridge University Press

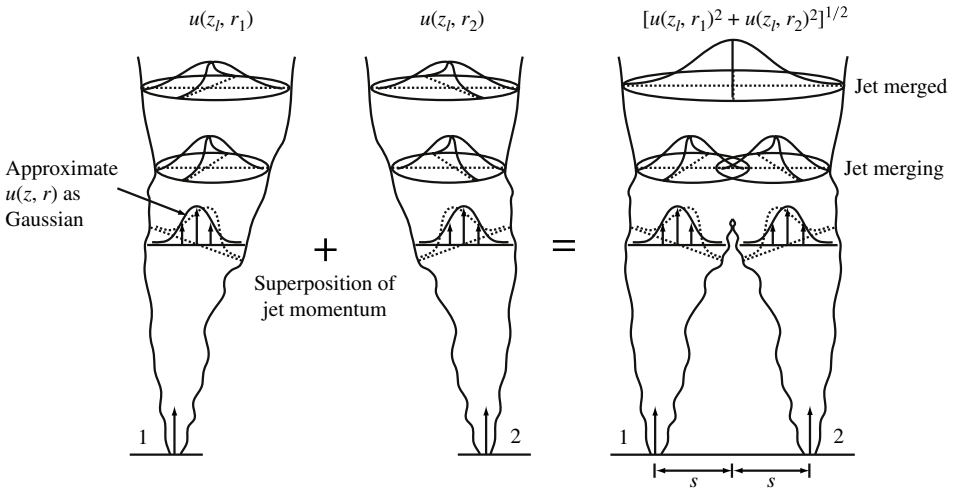


FIGURE 6. Momentum superposition for the velocity field of two interacting jets. Here r_1 and r_2 are the radial distances from the deflected jet centreline of jet 1 and jet 2, respectively.

Moawad & Rajaratnam 1999). The tracer concentration of merged jets and plumes $c_{N_J}(x, y, z_l)$ can then be obtained by the superposition of tracer mass flux with a known $u_{N_J}(x, y, z_l)$ by

$$c_{N_J} = \frac{\sum_{i=1}^{N_J} u_i c_i}{u_{N_J}}. \tag{3.3}$$

Equations (3.1) and (3.2) together with (3.3) can then be used to obtain the velocity and concentration of a jet or plume group. The approach is valid from the discharge point when jets are far apart up to the limit of the flow domain of interest where the jets are fully merged. The above momentum, tracer mass and kinetic energy superposition model for jets and plumes, respectively, are independently supported by detailed CFD computations of multiple jets and plumes (see appendix B for superposition of momentum, appendix C for kinetic energy and appendix D for tracer mass). It can also be shown that the superposition solutions give correct asymptotic behaviour of multiple jet and plume discharges (appendix E).

4. Comparison of model predictions with experiments of jets and plumes

The model is first tested against experimental data of two flows representative of the asymptotic limiting cases of a forced buoyant jet: the mixing of a clustered momentum jet group (Baines & Keffer 1974) and the coalescence of two turbulent axisymmetric plumes (Kaye & Linden 2004). It is well known that a forced turbulent buoyant jet ($Fr > Fr_p$) behaves like a momentum jet close to the source ($z/l_s \ll 1$), and develops into a plume far away ($z/l_s \gg 1$), where $l_s = M_o^{3/4}/\sqrt{F_o}$ is a jet momentum to buoyancy length scale (e.g. Fischer *et al.* 1979).

4.1. *Clustered jet group*

In the experiments of Baines & Keffer (1974), a cluster of 19 concentric vertical round air jets with $D = 0.003\,55$ m are discharged into a stagnant ambient fluid in the $+z$

https://doi.org/10.1017/jfm.2012.332 Published online by Cambridge University Press

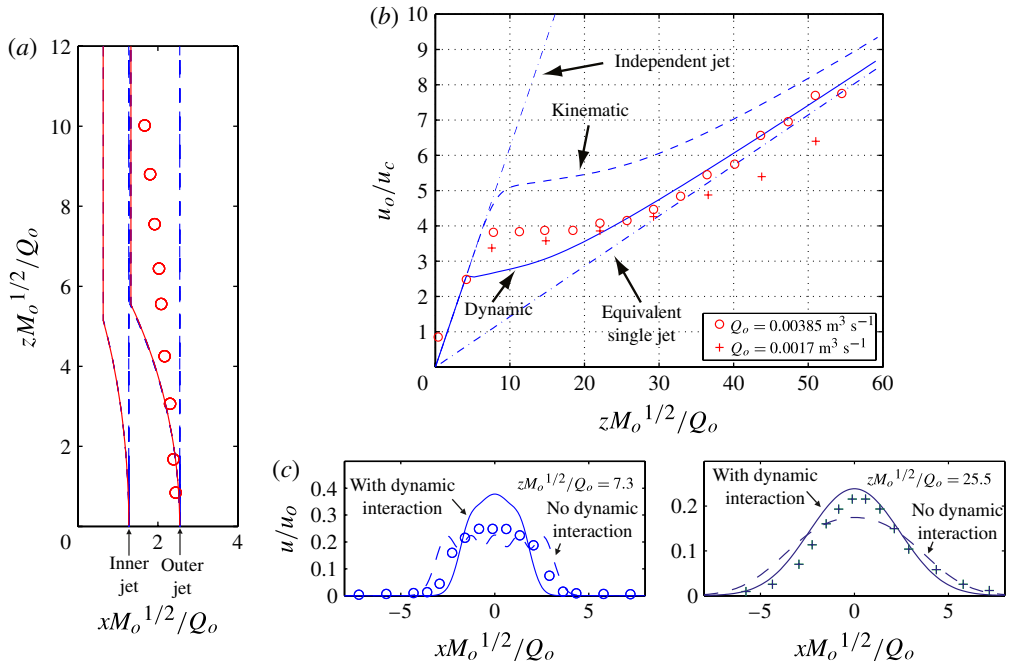


FIGURE 7. (Colour online) Comparison of predicted and observed jet mixing for the clustered jet group experiments of Baines & Keffer (1974): (*a*) inner and outer jet trajectories; (*b*) centreline velocity of jet group; and (*c*) transverse velocity profiles of jet group.

direction at room temperature; the locations of the jet nozzles in the source plane are shown in figure 5(*a*). The jet group consists of a central jet, an array of six jets equally spaced along the circumference of an inner circle (radius = 0.01745 m), and a second array of 12 jets on an outer circle (radius = 0.0349 m). The mean velocity field in the jets was measured along the line of symmetry (passing through five jets) at a number of horizontal sections above the source. Two different flow rates were tested, 0.003 85 and 0.001 70 m^3 s^{-1}. It was observed that the 19 jets tend to propagate towards one another due to mutual attraction, resulting in an apparent slow growth in the overall width of the jet group. The jet mixing is noticeably different from that of an isolated individual jet, or an equivalent round jet.

The three control volumes chosen for the model computation are shown in figure 5(*a*); by symmetry only the merging of four jets needs to be studied. The computed jet trajectories for the inner and outer jets along the line of symmetry are shown in figure 7(*a*). Jet merging is assumed to occur when the edge of a jet (defined by b_g) intersects with the edge of its adjacent jet in its deflecting direction; the subsequent composite jet is assumed to be vertical. Four iterations are typically required for the solution to converge. The computation shows that the outer jet deflects inwards noticeably; the inner jet also shows a deflection but to a lesser extent (by symmetry the centre jet trajectory is vertical). The predicted trajectory for the outer jet is in reasonable agreement with the measured centreline trajectory of the outer jet. In the model computations, the top boundary is assumed to be 230D, which is deduced from the measurement end points.

The predicted and observed centreline velocity decay of the jet group are shown in figure 7(*b*). It is seen that the jets are independent of each other near the source, up to about $z = 5M_o^{1/2}/Q_o$. Beyond this point the jet group appears to enter a 'zone of small

https://doi.org/10.1017/jfm.2012.332 Published online by Cambridge University Press

entrainment' as described by Baines & Keffer (1974), in which the centreline velocity is almost a constant. After jet merging, the centreline velocity decreases again.

Additional insight can be obtained by comparing the predicted centreline velocity of the jet group with the solutions of four limiting cases: (i) independent round jet treated as if there were no other jets; (ii) equivalent single jet that represents the jet group with the same total momentum and volume fluxes; (iii) kinematic superposition, with the jet interaction modelled by momentum superposition of straight jets (i.e. neglecting jet deflection); and (iv) the solution of the present dynamic jet interaction model, which accounts for the mutual attraction of jets. It is seen from figure 7(*b*) that superposition alone appears to be insufficient to describe the jet interaction. The zone of small entrainment and velocity decay can be satisfactorily predicted only by taking into account the jet deflection, which has a noticeable effect on the jet group mixing characteristics. Beyond about $z = 30M_o^{1/2}/Q_o$, the jet group can roughly be regarded as an equivalent single jet, as the jets have nearly merged completely. Note that the momentum superposition method is able to account for the transitional region between the unmerged and fully merged regions of multiple jets. Both the kinematic and dynamic interaction models predict correctly the clustered jet group to behave as an equivalent single jet asymptotically, but the height at which the single jet behaviour begins is more accurately predicted by the dynamic interaction model. Figure 7(*c*) shows that the effect of the interaction on the velocity field at different sections is also reasonably predicted.

The jet merging process can be visualized by the computed velocity field contour at different z level as shown in figure 8. For $z < 2M_o^{1/2}/Q_o$, the 19 independent jets can be clearly seen. For $z = 5M_o^{1/2}/Q_o$, jets start to merge with each other and each individual jet cannot be clearly distinguished. At about $z > 10M_o^{1/2}/Q_o$ the jets have merged to become a Gaussian-like profile that resembles a single jet discharge. At about $z > 25M_o^{1/2}/Q_o$, the jets have completely merged and appear to grow at a rate similar to an equivalent single jet.

4.2. *Turbulent plume pair*

Kaye & Linden (2004) conducted experiments to study the merging of a pair of axisymmetric turbulent plumes. The two vertical round plumes are spaced s (in their notation, which is different from our use of s to denote streamwise coordinate in § 2.2) apart and discharge in the $+z$ direction with initial volume flux Q_o, specific buoyancy flux F_o and negligible momentum flux M_o. Experiments were performed with equal source buoyancy flux ($F_{o1} = F_{o2}$), as well as unequal source fluxes (buoyancy flux ratio $= \Phi = F_{o2}/F_{o1}$, where F_{o1} is the stronger plume). The concentration field was measured with a light-induced fluorescence technique.

The model predictions are generated using average values of the governing parameters covered in experiments (Kaye & Linden 2004), with $D = 5$ mm, $Q_o = 1.5$ cm^3 s^{-1}, $g'_o = 90$ cm s^{-2} and $s = 2.5$–7.5 cm. The water depth is taken as 180 cm for equal-plume experiments and 35 cm for unequal-plume experiments. The control volume is chosen as shown in figure 5(*b*). Plume merging is assumed to occur when the edge of a plume (defined by b_g) intersects with the edge of its adjacent plume in its deflecting direction; the subsequent composite plume is assumed to be vertical. Five iterations are typically required for the solution to converge. For unequal-plume experiments, Q_o is multiplied by Φ to obtain the required buoyancy flux ratio while g'_o is kept constant; the weaker plume's densimetric Froude number Fr ($= u_o/\sqrt{g'_o D}$) changes by a factor of Φ as a result.

https://doi.org/10.1017/jfm.2012.332 Published online by Cambridge University Press

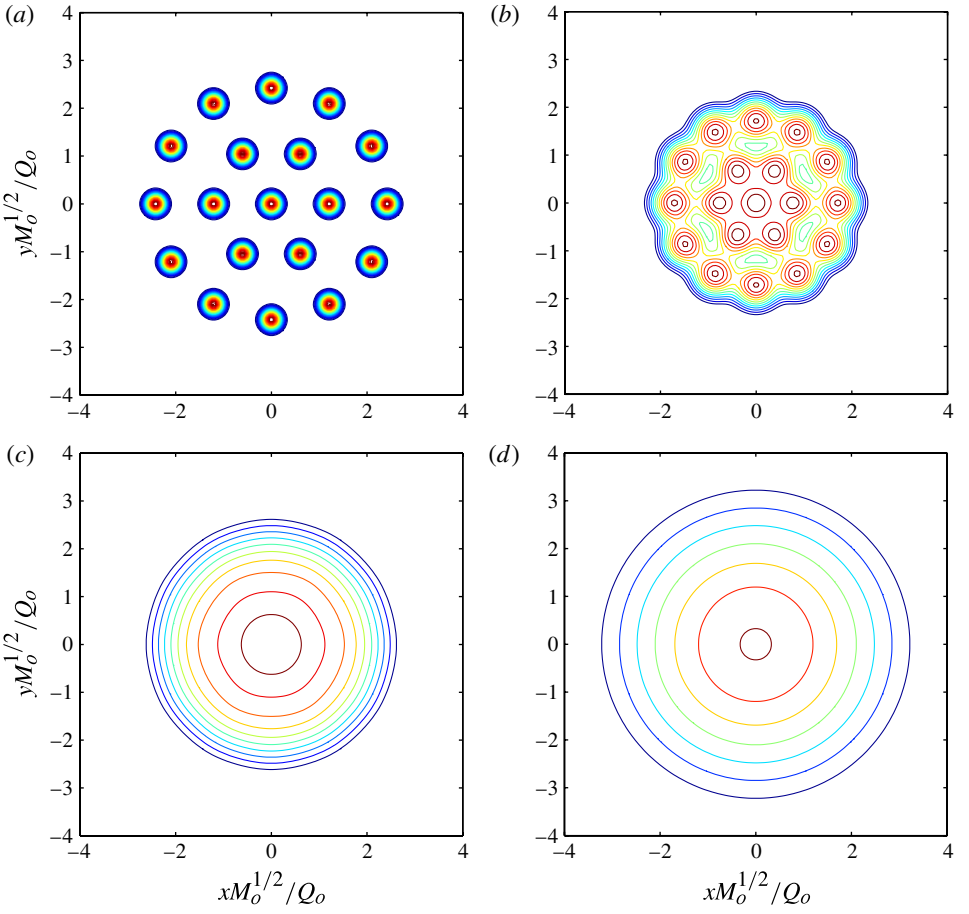


FIGURE 8. Predicted cross-sectional velocity field contours in u/u_c for the clustered jet group experiments of Baines & Keffer (1974) (contour level 0.1–0.8; step 0.02) for various $zM_o^{1/2}/Q_o$ values: (*a*) 2; (*b*) 5; (*c*) 10; and (*d*) 25.

4.2.1. *Equal plumes*

The entrainment field and reduced pressure between the two equal plumes (with equal buoyancy fluxes) result in a symmetrical mutual attraction, which draws the plumes towards each other and leads to a lower merging height than if there were no such attraction. Until the merging has taken place, the lateral concentration or buoyancy profile will indicate two distinct peaks. As in the experiments, the merging height is defined as the level when the plumes have sufficiently merged to result in only one peak on the centreline of the lateral buoyancy profile (Kaye & Linden 2004).

The predicted concentration contours in the plane of symmetry of an equal-plume pair is shown in figure 9(*a*), which shows that both plumes deflect to the same extent. The comparison between predicted and observed merging height for equal plumes is shown in figure 9(*b*) along with the prediction if plume interaction is not taken into account. As the plume initial spacing increases, the merging height increases almost linearly; model predictions are in good agreement with observations. It is seen that the merging height will be significantly over-predicted if dynamic interaction is not considered.

https://doi.org/10.1017/jfm.2012.332 Published online by Cambridge University Press

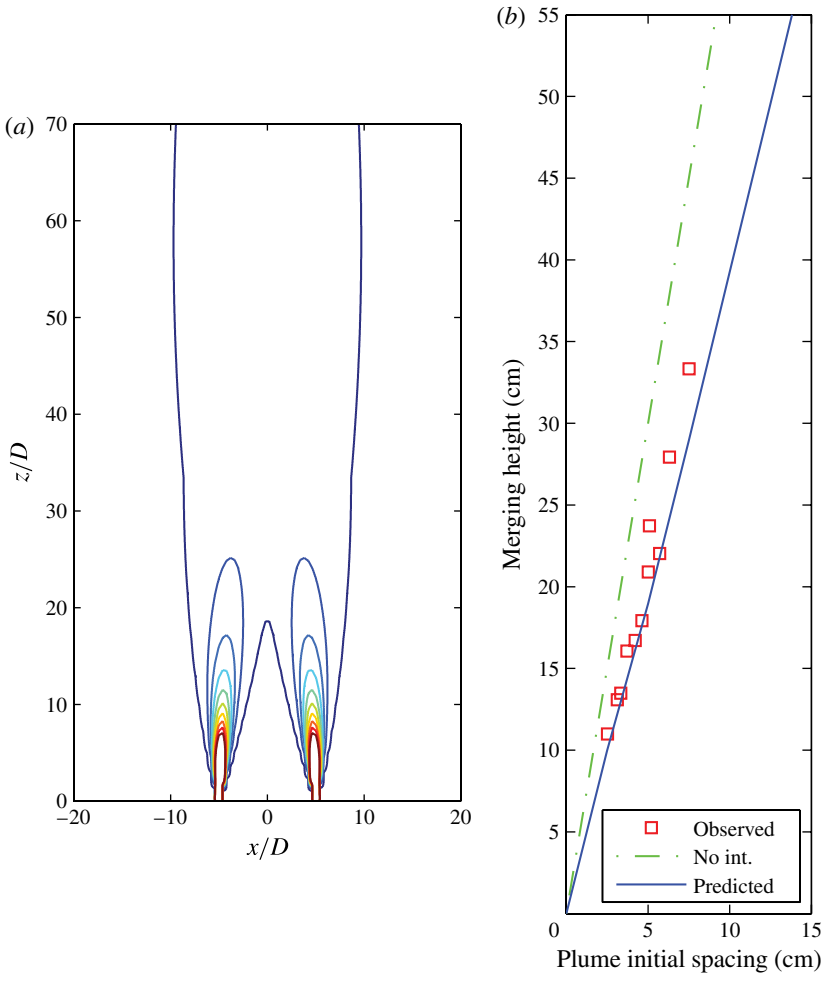


FIGURE 9. (Colour online) (*a*) Predicted concentration field ($\Phi = 0.1$; $c/c_o = 0.005$–0.365 with interval 0.04) and (*b*) comparison of predicted and observed merging height of equal-plume pairs.

4.2.2. *Unequal plumes*

An unequal-plume pair refers to the discharge of two plumes with different buoyancy fluxes. Figure 10(*a*) shows the predicted concentration contours of an unequal-plume pair with $\Phi = 0.1$. As the plume entrainment velocity is proportional to $F_o^{1/3}$, the stronger plume (left) with 10 times greater buoyancy flux induces a stronger but not proportional entrainment flow. It is seen that the weaker plume (right) is deflected towards the stronger plume. Figure 10(*b*) shows the comparison of merging height of an unequal-plume pair as a function of buoyancy flux ratio with the data of Kaye & Linden (2004). For unequal plumes, the occurrence of a buoyancy peak on the centreline is no longer an appropriate criterion for merging; it is equivalently defined as the location for the disappearance of the trough in the buoyancy profile. The predicted merging height shows a steep increase from $\Phi = 0.0$ to 0.2; from $\Phi = 0.2$ to 0.5 the increase begins to level off; and from $\Phi = 0.5$ onwards the increase is insignificant. It is seen that the predicted variation of merging height with Φ is in good agreement with the data. Predictions with plume boundaries defined at

https://doi.org/10.1017/jfm.2012.332 Published online by Cambridge University Press

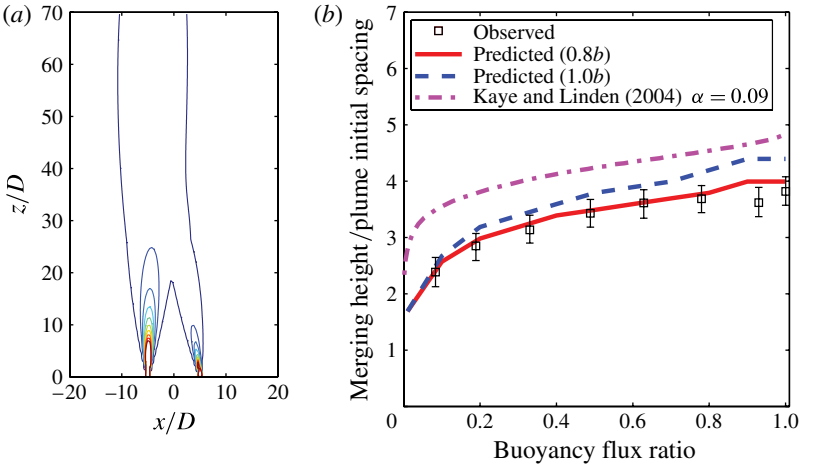


FIGURE 10. (Colour online) (*a*) Predicted concentration field ($\Phi = 0.1$; $c/c_o = 0.005$–0.365 with interval 0.04) and (*b*) merging height as a function of buoyancy flux ratio of unequal-plume pairs (symbols represent measurement data and error bar limits reported in Kaye & Linden 2004).

$0.8b_g$ show good agreement with the data (b_g = Gaussian plume half-width); defining the boundary at b_g slightly over-predicts the merging height, but the comparison is still reasonable considering the scatter in the data. Using a well-established plume entrainment coefficient of $\alpha = 0.09$, the model of Kaye & Linden (2004) significantly over-predicts the merging height.

5. Rosette buoyant jet group: experiments and modelling

In a rosette buoyant jet group, the jets are typically discharged horizontally around the circumference of a riser with diameter D_R (figure 1*b*). This Bunsen burner-type arrangement maximizes the mixing with the environment. Previous studies have observed that the buoyant jets tend to deflect towards each other as they rise and merge to form a single rising column above the source. This problem is considered most complex, as it involves inclined buoyant jet discharges, varying local densimetric Froude number and varying entrainment coefficient.

5.1. *Experiments*

Experiments are carried out to investigate the dynamic interaction of a rosette buoyant jet group in a 12 m by 5 m wide shallow water basin; the water depth is set at 0.65 m. The discharge is measured by a calibrated rotameter. The required buoyant source fluid was prepared by mixing predetermined amounts of ethanol and water. Densities of the source fluid and the ambient are measured using a precision density meter.

Three series of experiments of $Fr = 1.2$, 2.5 and 4.9 are carried out; the jet diameter is $D = 0.49$ cm, and the riser diameter is $D_R = 5.6$ cm. For each Fr the initial relative density difference and flow rate $Q_o = 5$–20 l h^{-1} are kept constant, and the jet interaction is studied for different number of jets, $N_J = 1$, 2 and 6. The jet Reynolds number $Re = u_o D/\nu$ lies in the range 400–1500, where ν is the kinematic viscosity of water. The resulting jet trajectory is captured using the laser-induced fluorescence (LIF) technique. A laser sheet of approximately 5 mm thickness is generated by a 5 W argon-ion laser source and cut through the centreline plane of a jet group; the resulting image is captured by an underwater charge-coupled device (CCD) camera.

https://doi.org/10.1017/jfm.2012.332 Published online by Cambridge University Press

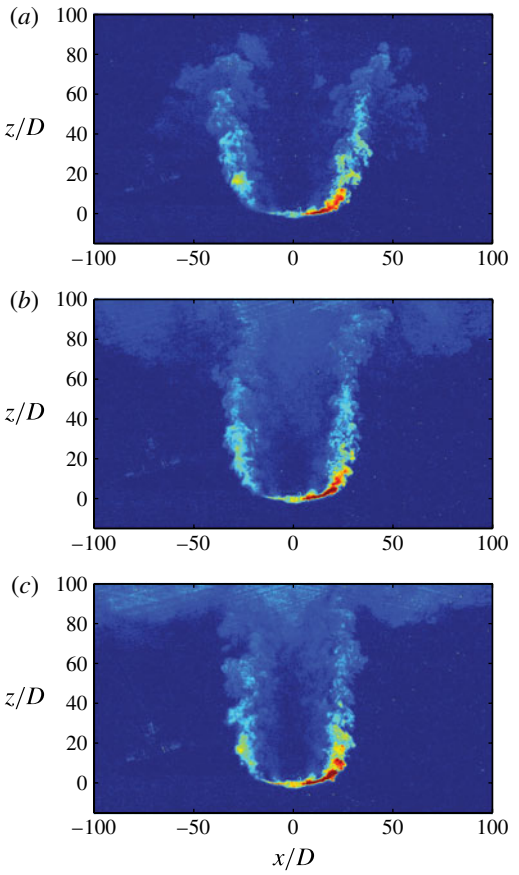


FIGURE 11. LIF images in the centreline plane of a rosette jet group discharge ($N_J = 6$) for $Fr \approx 7.4$ at times: (*a*) $t = 15$ s; (*b*) $t = 30$ s; and (*c*) $t = 60$ s.

Four-hundred LIF images (576 × 768 pixels) are taken at a time interval of 0.1 s; these images are time-averaged for further analysis. By symmetry, only one of the N_J jet trajectories is needed, so as to maximize the image resolution covered by each jet. The time-averaged image is background-subtracted. The resulting image shows a jet trajectory with sharp boundaries. The centreline trajectory of the jet is defined as the mid-point between the two jet boundaries (defined by the $c/c_o = 0.05$ contour).

Additional experiments (with $Fr = 7.4$) are also carried out in a 3 m × 0.3 m × 0.76 m deep glass tank for study of the interaction process. The mixing of buoyant jets in the plane of the laser sheet is visualized and video-recorded by a Sony HDR-FX7E video camera recorder. About 1 min of the recorded video is converted to a series of photos (1080 × 1920 pixels) at three frames per second. This series of photos was time-averaged and background-subtracted to produce the final image. Details of the experimental set-up and measurement technique can be found in Lai (2009) and Lai, Yu & Lee (2011).

5.2. *Jet merging*

Significant dynamic interaction is observed in the experiments. The jet interaction in the plane of symmetry of a six-jet group is illustrated in figure 11 with $D = 0.49$ cm,

https://doi.org/10.1017/jfm.2012.332 Published online by Cambridge University Press

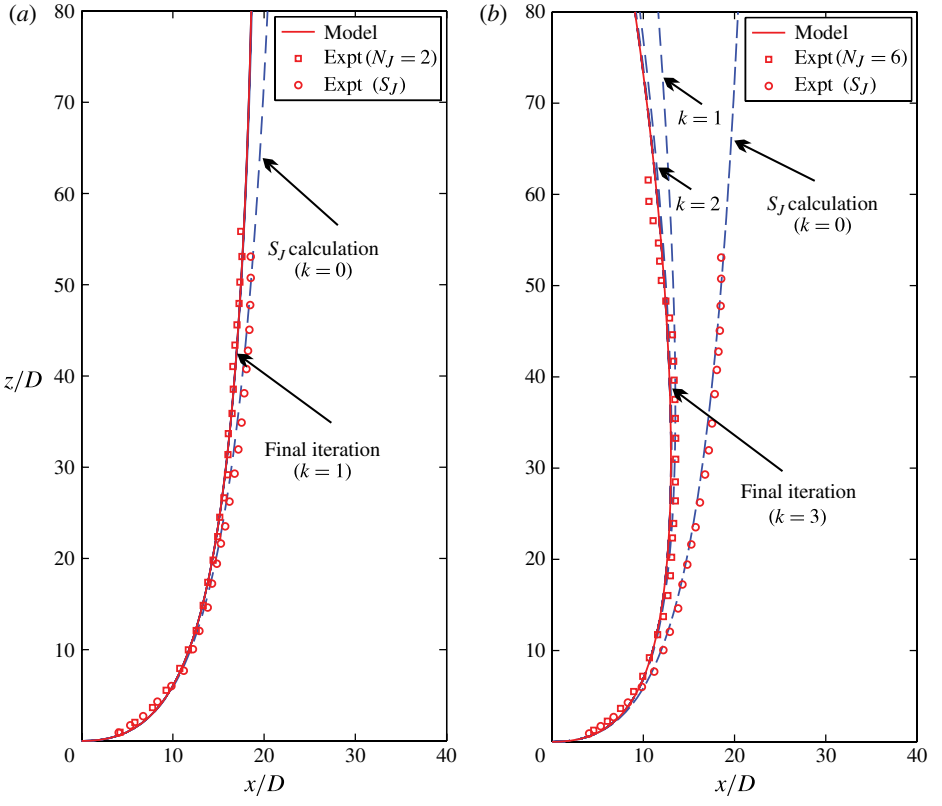


FIGURE 12. (Colour online) Comparison of predicted and observed jet trajectories of a rosette buoyant jet group: (*a*) $N_J = 2$ and (*b*) $N_J = 6$ ($Fr = 4.9$). S_J: single jet.

$D_R = 5.6$ cm, $u_o = 0.365$ m s^{-1} and $Fr = 7.4$. Shortly after discharge, the jet on one side travels as if other jets do not exist, and the dynamic interaction is not apparent (figure 11*a*). After the jet impinges on the free surface, the mixed fluid in the buoyant surface layer is split into two streams – a part travelling away from the centreline and another part moving towards the centre plane to join the surface layer formed by the jets on the opposite side. The mixed fluid at the centre then descends and is re-entrained into the jet group or rises back to the surface due to its remaining buoyancy (figure 11*b*). The jets from the two sides then gradually bend towards each other, and a final quasi-steady flow is eventually formed (figure 11*c*). Owing to the blockage of the laser sheet by the riser, the trajectory at the left-hand side appears to have a lower concentration than that of the right-hand side in the LIF images; the observed jet trajectory that is not affected by the blockage is used for analysis.

5.3. *Comparison of model predictions with experiments*

For a six-jet group, the control volume is chosen with two planes of symmetry and a circular arc far from the jet (figure 5*c*). The jet trajectory is computed (typically three or four iterations are required) until the outer edges of adjacent jets (defined by b_g) intersect. Both the free and bottom surface have been accounted for using the method of images. A contraction coefficient of 0.80 (for nozzle area) is adopted based on best-fitting the observed single free buoyant jet trajectory with the integral jet model prediction. Figure 12 shows the comparison of predicted and observed jet

https://doi.org/10.1017/jfm.2012.332 Published online by Cambridge University Press

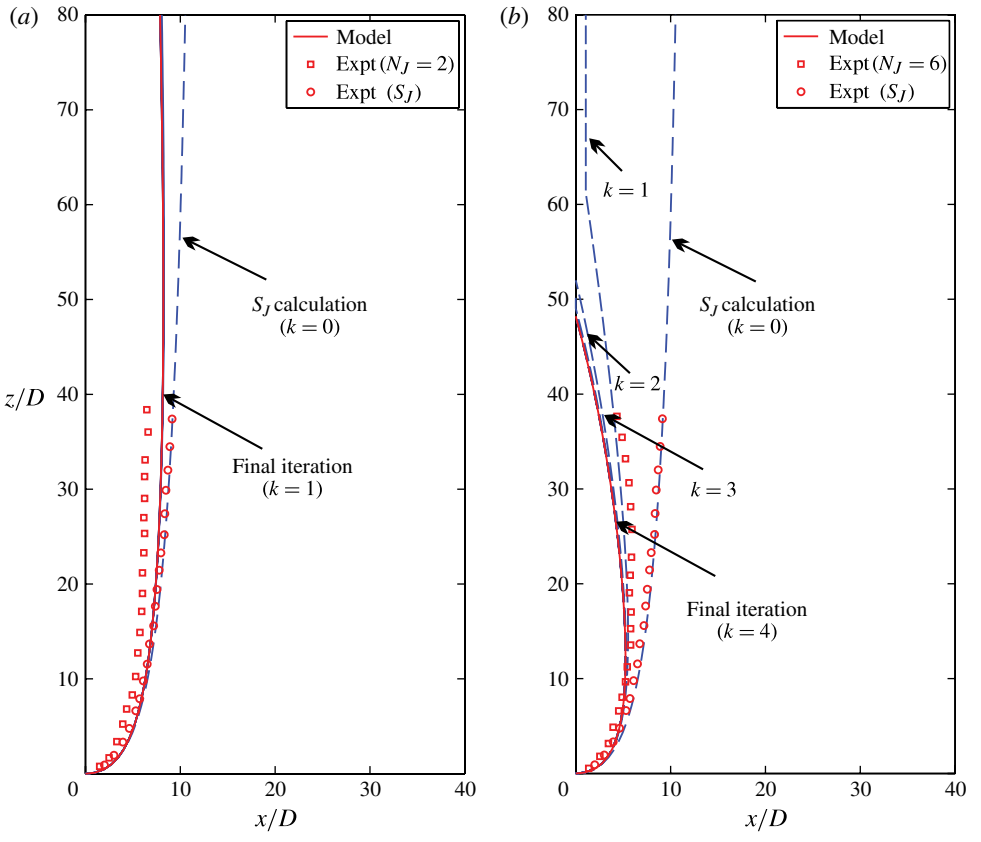


FIGURE 13. (Colour online) Comparison of predicted and observed jet trajectories of a rosette buoyant jet group: (*a*) $N_J = 2$ and (*b*) $N_J = 6$ ($Fr = 2.5$).

trajectories of (*a*) two-jet and (*b*) six-jet rosette buoyant jet groups. It can be seen that, for $N_J = 2$, the jet deflection is small compared to a single free jet; for a six-jet group the jet interaction is significant. Also shown are the intermediate iterations during the computation. When interaction is weak ($N_J = 2$), the solution converges quickly with only one iteration; more iterations are needed for cases with stronger interaction ($N_J = 6$). Similar comparisons can be found for an experiment with $Fr = 2.5$ (figure 13). In general the prediction is in good agreement with experimental data.

Figure 14 shows the induced velocities at the centreline plane ($N_J = 6$). It can be seen that, if the interaction is not taken into account, the merging would occur much later. The pressure and entrainment fields at $z = 20D$ show that jets would be well-separated if jet interaction were not taken into account (figure 15).

The model predictions are also compared with the rosette jet group data of Seo *et al.* (2004) and Kwon (2005); their experiments were carried out using heated jets and at generally higher Fr (≈6–13). The observed inward deflection of the jet trajectory, and the stronger interaction with increasing number of jets for the same Fr are well predicted (figure 16).

Dynamic interaction of rosette buoyant jet groups has also been investigated experimentally in physical model studies of the Boston outfall by Roberts & Snyder (1993*a*,*b*). The flow is discharged horizontally from a number of risers mounted on

https://doi.org/10.1017/jfm.2012.332 Published online by Cambridge University Press

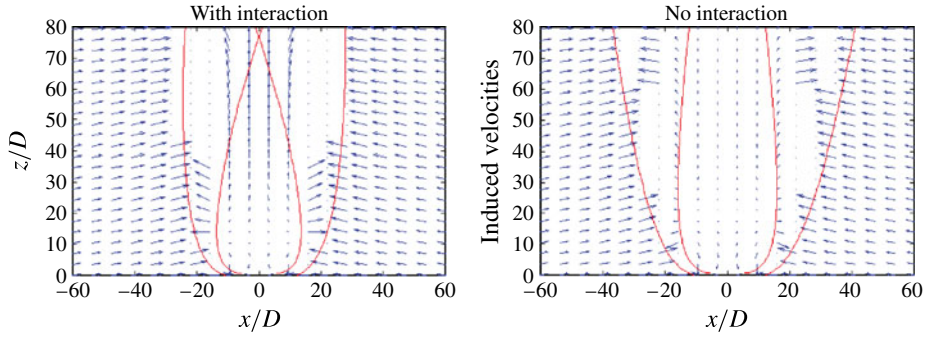


FIGURE 14. Rosette jet group induced velocities at centreline plane ($N_J = 6$; $u_o = 0.365$ m s^{-1}; $Fr = 4.9$). Red lines indicates buoyant jet boundaries.

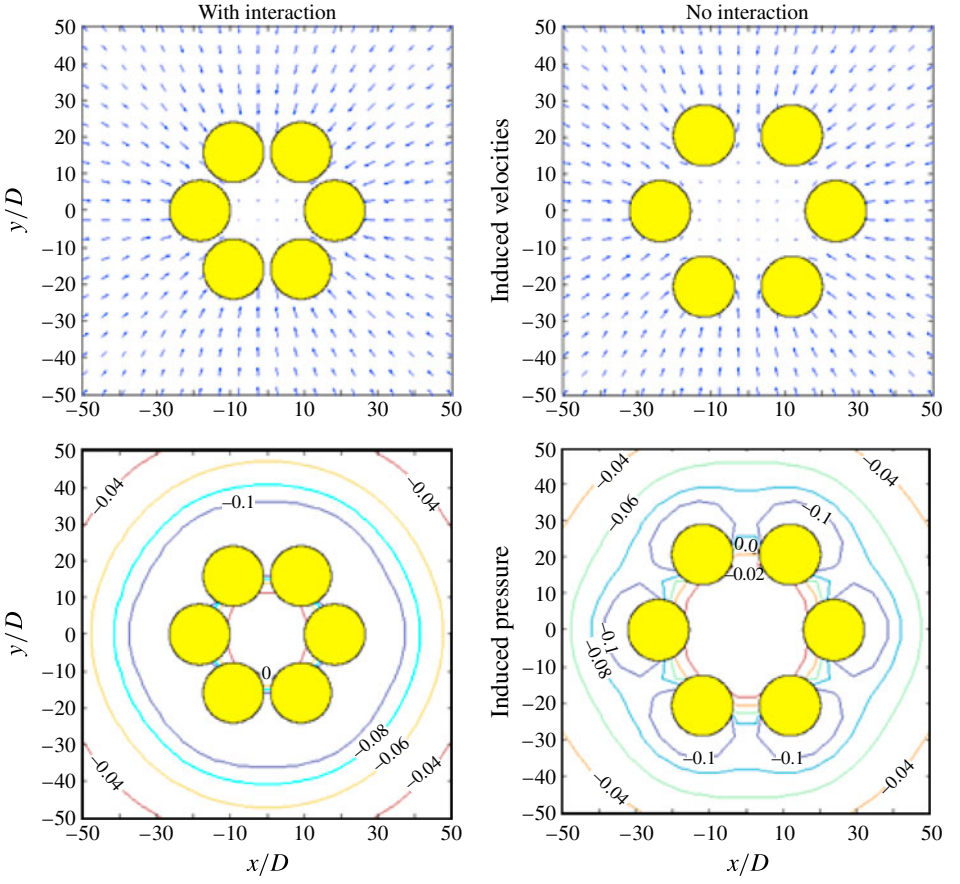


FIGURE 15. Rosette buoyant jet group induced velocity and pressure field at a horizontal cross-section at $z = 20D$ ($N_J = 6$; $u_o = 0.365$ m s^{-1}; $Fr = 4.9$).

an ocean outfall; for each riser, N_J jets discharge as a rosette jet group. For a given total volume, momentum and buoyancy flux from each riser, it was observed that

https://doi.org/10.1017/jfm.2012.332 Published online by Cambridge University Press

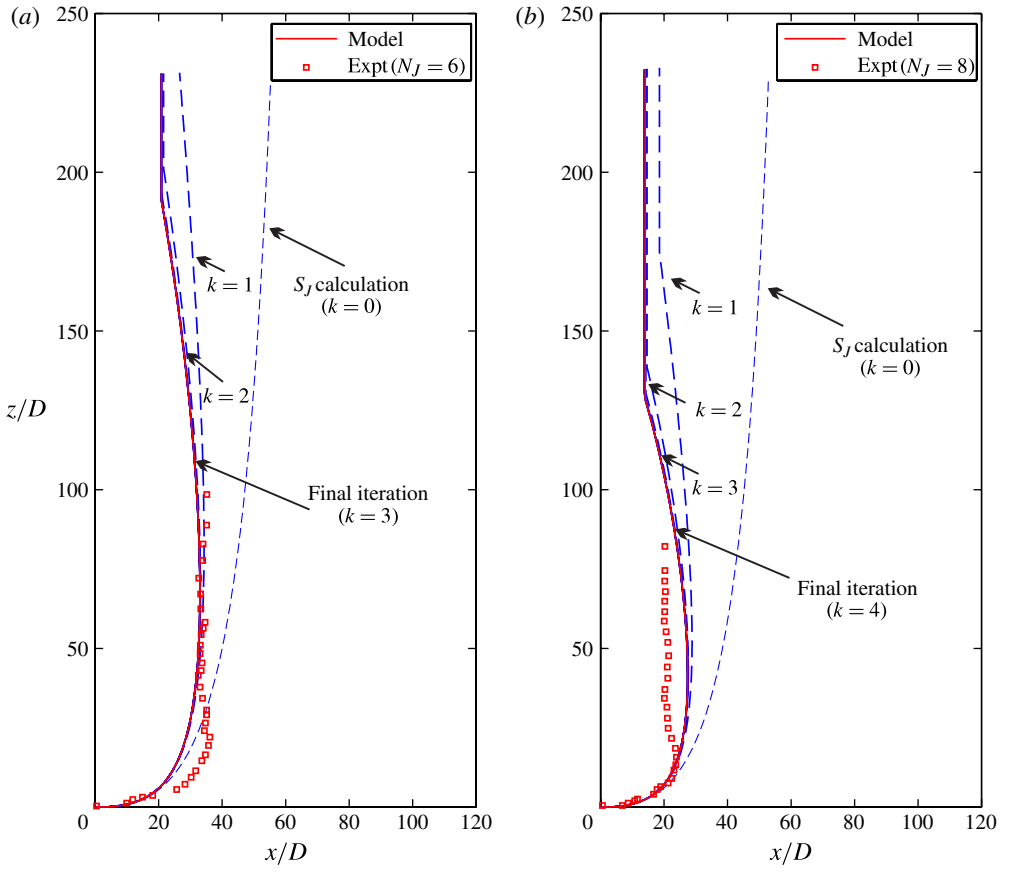


FIGURE 16. (Colour online) Comparison of predicted and measured trajectories of a rosette buoyant jet group of Kwon (2005): (*a*) $N_J = 6$ and *b*) $N_J = 8$ ($Fr \approx 13$).

the interaction of a 12-jet group ($N_J = 12$) was stronger than that of an eight-jet group, resulting in a narrower jet group spreading width. The present model is used to predict the spread of the jet group for a single riser ($D_R = 3$ m). A jet diameter of $D = 0.157$ and 0.130 m (prototype scale) were used for the eight- and 12-jet group, respectively, with $Q_o = 0.311$ m^3 s^{-1} per riser and $Fr \approx 10$. The ambient density was nonlinearly stratified with density profile given in Roberts & Snyder (1993*a*). Figure 17(*a*) shows the spread of the eight-jet jet group with and without interaction; for this case the interaction appears not to be strong enough to produce a significant difference. Figure 17(*b*) shows the spread of a 12-jet group. It can be seen that with the same flow discharge the stronger jet interaction tends to pull in the outer jets; the contraction of jet group results in an apparent lack of growth of the jet group – much like what was noted by Baines & Keffer (1974) from their velocity measurements. The computed entrainment flow and pressure fields at $z = 10$ m (figure 18) clearly demonstrate the much stronger mutual attraction among the jets for $N_J = 12$ compared to that in the eight-jet group. As the physical model study was mainly concerned with measurement of the maximum concentration (dilution), the lack of details of the flow visualization and measured jet trajectories does not permit a more extensive quantitative comparison.

https://doi.org/10.1017/jfm.2012.332 Published online by Cambridge University Press

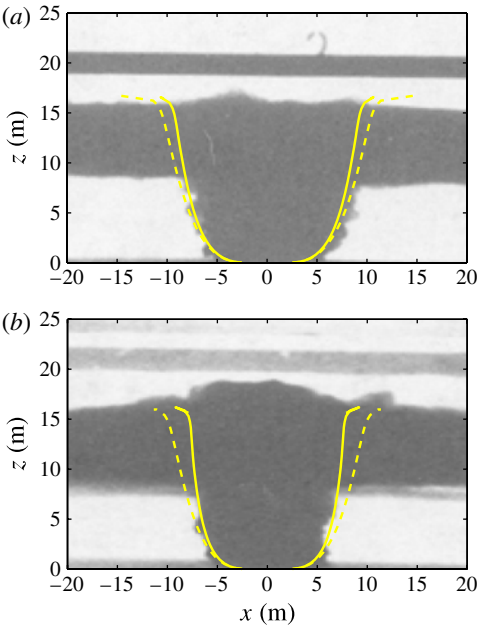


FIGURE 17. (Colour online) Comparison of the spread of rosette buoyant jet group with observation in a physical model of the Boston outfall (Roberts & Snyder 1993*b*): (*a*) $N_J = 8$ and (*b*) $N_J = 12$ ($Fr \approx 10$); with interaction (solid line); no interaction (dashed line).

5.4. *Stability and uniqueness of multiple buoyant jet flows*

The foregoing theoretical development has tacitly assumed a stable and unique swirl-free multiple jet flow configuration, and symmetry arguments have been used in the numerical solution. For example, a buoyant jet emanating from the centre of the base of a box does not necessarily have a unique arrangement; the jet can be attracted to any of the box walls depending on small differences in the initial conditions of the source flow. This issue can be addressed both experimentally and in relation to previous work on confined buoyant jets. First, we did not observe any instability in any of our rosette jet group experiments for various configurations in both stagnant or flowing ambient fluid (Lai & Lee 2012). Second, extensive physical model experiments on such rosette buoyant jet groups have been carried out (e.g. Roberts & Snyder 1993*a*,*b*), and jet instability was not reported. Third, this instability issue was also not reported in the experiments on clustered jet group experiments (Baines & Keffer 1974) or interaction of plume pairs (Kaye & Linden 2004).

Under certain situations a buoyant jet discharge may not have a unique or stable flow configuration. Consider a vertical round buoyant jet of diameter D discharging at the bottom of a cylindrical riser of diameter D_r and height H_r. Experiments showed that the effect of the lateral confinement can be represented by a confinement index $\beta = H_r/(D_r - D)$ (Lee & Lee 1998). It was found that, for $\beta \leqslant 1.5$, the confinement has no effect. For $1.5 < \beta \leqslant 3$, it was observed that the buoyant jet was always deflected and attached to the sidewall of the riser instead of remaining on the axis of symmetry. Once this instability occurs, the plume remains attached to the wall and swirls around within the riser at a distinct frequency. For $\beta > 3$ the jet is significantly confined. The swirl is not observed; however, there is almost full mixing of the

https://doi.org/10.1017/jfm.2012.332 Published online by Cambridge University Press

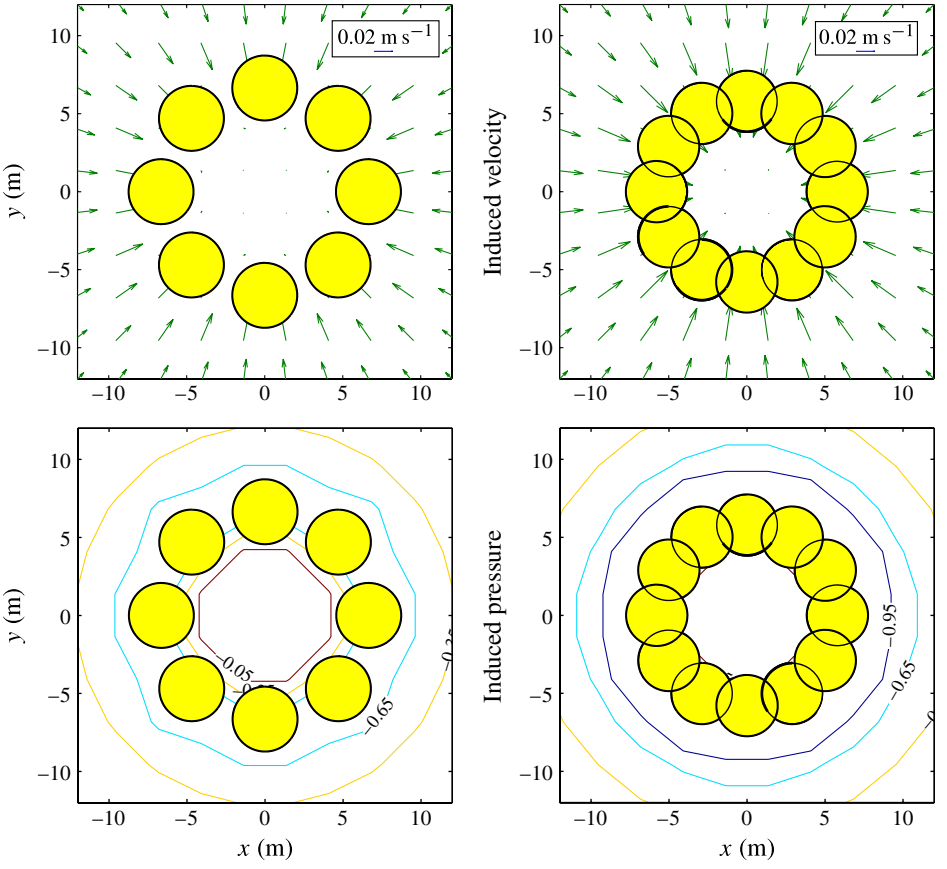


FIGURE 18. Rosette buoyant jet group induced velocity and pressure field at a horizontal cross-section ($z = 10$ m) in a physical model of the Boston outfall (Roberts & Snyder 1993*b*).

jet with the fluid inside the riser as it rises by virtue of its initial momentum and buoyancy.

For the flows under consideration, the jet discharge is not confined laterally by any solid boundary. However, we can obtain a conservative estimate of the confinement effect due to the presence of other buoyant jets using the above result. To illustrate, for the case of the 19 clustered jet discharges (Baines & Keffer 1974), we assume the central jet to be confined within a 'cylinder' with diameter half the size of the inner circle of figure 5(*a*). The corresponding jet confinement can be evaluated as $D = 0.003\,55$ m, $H_r \approx 0.0174$ m (before touching adjacent jets) and $D_r \approx 0.017\,45$ m, giving $\beta = 1.25$, suggesting that the clustered jet flow falls in the stable regime. For the rosette jet group configuration, the jets are even less confined ($H_r \sim D_r$ and $D/D_r \sim 0.1$ or less) and should also be expected to fall in the stable regime.

A swirling buoyant jet is typically produced by inducing the circulation or swirl at source (through the shape of the jet nozzle or other means). For our problem there is no angular momentum or external force imparted to the jet discharge at source; considering the magnitude of the jet entrainment velocity (typically around 5 % of the jet characteristic velocity), it is not likely that significant swirl can be induced by the jet interaction. The lack of swirl is also borne out by the velocity measurements.

https://doi.org/10.1017/jfm.2012.332 Published online by Cambridge University Press

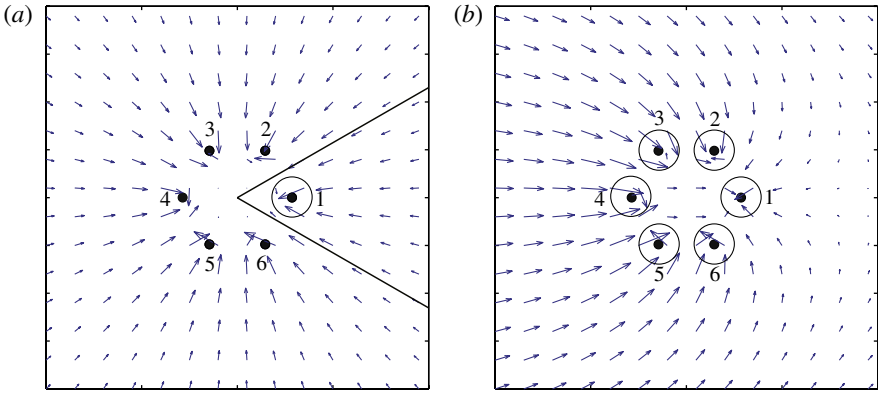


FIGURE 19. (Colour online) Computed external flow field induced by a rosette jet group in weak cross-flow: (*a*) stagnant ambient condition; and (*b*) cross-flowing ambient fluid. The local control volumes chosen for horizontal momentum balance are also shown.

Take, for example, the central jet in the 19 clustered jet experiment of Baines & Keffer (1974). It can be seen from figure 7(*b*) that initially the central jet behaves as an independent single jet, and its centreline velocity can be predicted by classical jet theory without swirl. If significant swirl is induced, it is expected that the jet characteristics would be significantly different (e.g. spread rate) from a jet without swirl (Pratte & Keffer 1972), which appears not to be the case here.

6. Dynamic interaction of buoyant jets in a cross-flow

The dynamic interactions of closely spaced multiple buoyant jet groups in a stagnant ambient have been investigated in the previous sections. The effect of an ambient current can be incorporated into the present model by adding the ambient velocity to the jet group induced velocity field. Equations (2.7)–(2.13) remain valid if the current is weak so that entrainment is close to that of the stagnant ambient (Gaskin 1995; Davidson, Gaskin & Wood 2002). The resultant flow field induced by the jet group and ambient current is unsymmetrical for each of the jets, and the momentum flux change due to this flow field is different for every jet. Momentum balance is thus carried out for every jet in the group.

The effect of an ambient current can be illustrated by an example, with six jets ($N_J = 6$, $D = 0.0044$ m) discharging horizontally on a riser (horizontal angle 0–2π, vertical angle 0), with $u_o = 0.365$ m s^{-1} and $\Delta\rho/\rho_a = 0.1266$, giving $Fr = 4.9$. Three ambient current speeds (U_a) are tested: $U_a = 0$, 0.03 and 0.08 m s^{-1}, giving a jet-to-ambient velocity ratio of $K = u_o/U_a = 4.6$–12.2. Water depth is 0.4 m.

For a rosette jet group in stagnant ambient fluid, a control volume can be chosen at the no-flux boundaries as shown in figure 19(*a*). When an ambient current is added, the external flow field is asymmetric (figure 19*b*). A local control volume used for each jet can be conveniently chosen to be a circle with boundaries in the external flow (just enclosing the jet, with radius $r = B = \sqrt{2}b_g$). Sensitivity tests have shown that the jet trajectory computation is not sensitive to the exact choice of an appropriately defined control volume (appendix F).

Figure 20 shows the comparison of the interacted jet trajectory and that without interaction for $U_a = 0.03$ and 0.08 m s^{-1}. The computation for that without interaction

https://doi.org/10.1017/jfm.2012.332 Published online by Cambridge University Press

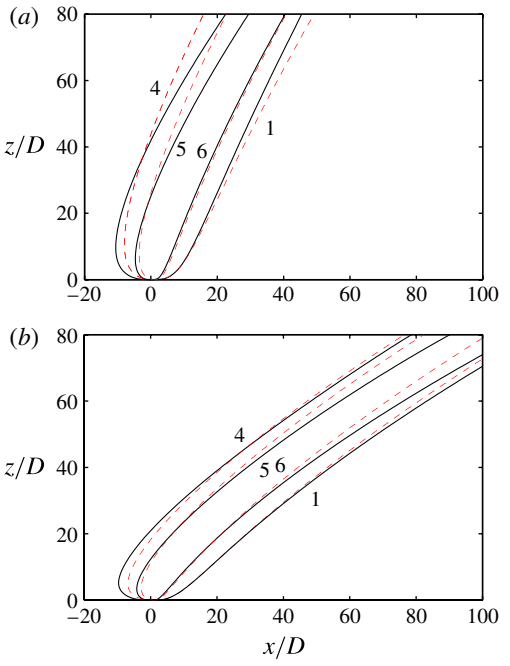


FIGURE 20. (Colour online) Comparison of the interacted (solid line) and non-interacted jet (dashed line) trajectory of a rosette jet group for two jet-to-ambient velocity ratios, $K = u_o/U_a$: (*a*) $K = 12.2$ and (*b*) $K = 4.6$. The numbers next to the jet trajectory refer to the individual jets labelled as in figure 19.

is done by solving (2.7)–(2.13) in the absence of other jets. Deflection of the interacted jets indicates the degree of interaction. Compared to the corresponding discharge in stagnant ambient fluid (figure 12*b*), it can be seen with the addition of a current that the degree of jet interaction tends to be less. The interaction is further reduced with increase of U_a: with a jet-to-ambient velocity ratio of $K = 4.6$, the interaction is so weak that the co-flow jet (jet 1) is not affected by the adjacent jets at all, as seen in figure 20(*b*); the interaction also decreases with increasing Fr.

For a single jet in weak cross-flow, the jet entrainment was shown to be unaffected and is approximately the same as that in stagnant ambient fluid (Gaskin 1995; Davidson *et al.* 2002). With this assumption, the deflection of a jet in a cross-flow is caused by: (i) the momentum imparted by the ambient current (without additional entrainment); and (ii) additionally the entrainment field induced by the other jets (if present), which is fixed for the same jet discharge configuration. The effect of (ii), i.e. from multiple jet discharges, would then be less important when (i) is increased. It should be kept in mind that the above computation serves mainly to demonstrate the decreased jet interaction in a current. For $K \lesssim 10$, the jet is bent over and there will be significant vortex entrainment – which is totally neglected in the present formulation. Despite the theoretical limitations, the essentially heuristic model computation is consistent with the recent experimental findings of Lai *et al.* (2011), which indicate that for typical jet-to-riser diameters of the order $D/D_R \approx 0.1$, dynamic interaction of a rosette buoyant jet group is negligible in a moderate cross-flow, and each jet can be treated independently without taking into account the dynamic interaction (i.e. only kinematic interaction of plume overlap needs to be considered).

https://doi.org/10.1017/jfm.2012.332 Published online by Cambridge University Press

7. Conclusions

Dynamic interaction of multiple buoyant jets in stagnant ambient conditions can be predicted by a semi-analytical model. The jet-induced external flow is computed by a distribution of point sinks along multiple free jet trajectories obtained using integral jet models based on a well-established shear entrainment hypothesis. The dynamic interaction is incorporated into the governing equations of a buoyant jet in an exact horizontal momentum balance using a control volume approach. The deflected jet trajectory is determined through the iterative solution of the external entrainment flow and the multiple buoyant jet trajectories. The mixing characteristics of the multiple jet group after merging are determined by superposition of local momentum (for jets) or kinetic energy (for plumes) and tracer mass (or buoyancy) flux.

The model is validated against data of past investigations as well as our own experiments. Predicted jet trajectories, velocity and tracer concentration are in good agreement with the experimental data for representative flows covering the jet–plume range: clustered turbulent jet groups, turbulent plumes discharging in proximity, and the mixing of a rosette buoyant jet group. The theory has also been applied successfully to jet discharges from alternating diffusers. The success of the present model indicates the importance of the exact determination of the pressure force and the momentum flux in the horizontal momentum balance. The superposition approach for modelling jet groups is also supported by 3D CFD solutions of the Reynolds-averaged Navier–Stokes (RANS) equations. In addition, numerical experimentation shows that the jet group velocity for a buoyant jet with both momentum and buoyancy (say $1 < Fr < 40$) can be obtained by interpolation between the jet-induced and the plume-induced jet group velocity (obtained from superposition of u^2 and u^3 respectively), in accordance with the local densimetric Froude number (similar to the computation of the local entrainment coefficient).

The model can be extended to treat a multiple jet group in a weak cross-flow; the theoretical results show that the interaction decreases as current speed increases. The theory can also be extended to treat multiple jets in a moderate to strong cross-flow using a Lagrangian model for a 3D buoyant jet in cross-flow that predicts the shear entrainment in the near field as well as the vortex entrainment due to the cross-flow (Lee & Chu 2003). The jet entrainment flow is modelled by a distribution of point sinks, and the blockage and sheltering effect by a distribution of doublets along the jet axis. For tandem jets in a cross-flow, it is observed that the most upwind jet is deflected most, and all the sheltered downstream jets are deflected less, and all to a similar degree. The predicted jet trajectories are all in good agreement with data Lai & Lee (2010).

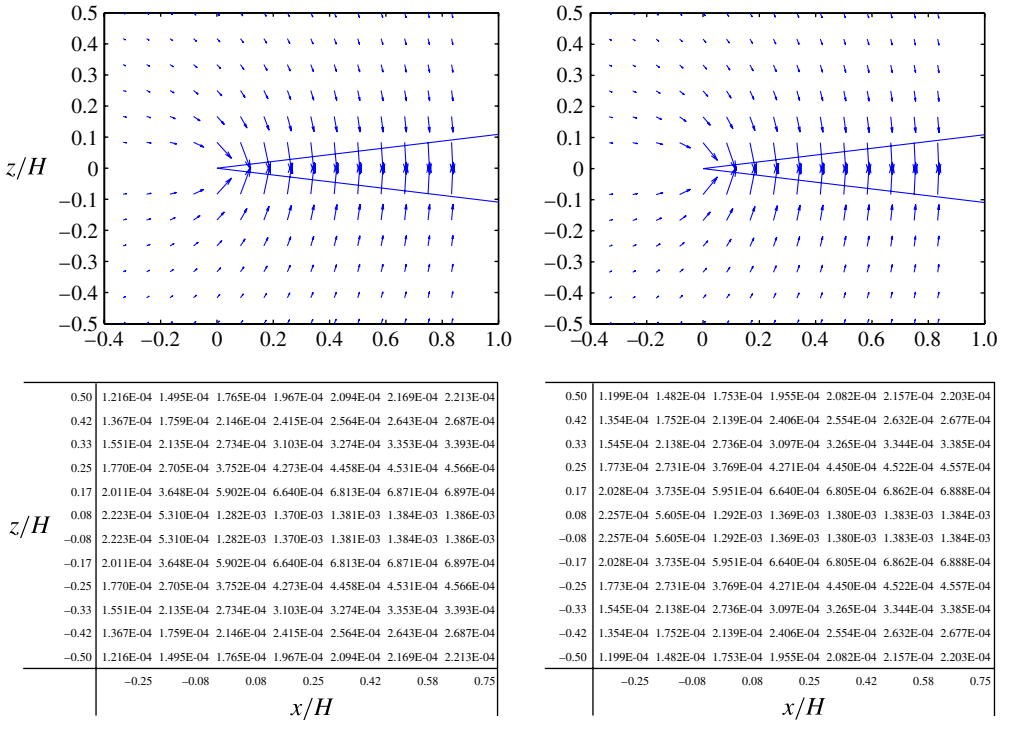
Acknowledgements

The authors wish to thank the Hong Kong Research Grants Council (Project No. HKU 7518/03) and the University Grants Committee (Project No. AoE/P-04/04) for their financial support of this research. The helpful comments and suggestions of the anonymous reviewers are gratefully acknowledged.

Appendix A. Computation of external flow induced by jets

Squire (1951) and Batchelor (1967) gave an exact analytical solution of a round laminar jet in stagnant fluid using a constant molecular viscosity. The field solution of the full Navier–Stokes equations covers both the jet and the external flow. Squire showed that the solution is also valid for a turbulent round jet of constant eddy

https://doi.org/10.1017/jfm.2012.332 Published online by Cambridge University Press



Taylor's solution Distributed point sinks

FIGURE 21. (Colour online) External flow at centreline plane induced by a turbulent round jet ($D = 0.1$ m; $u_o = 1.75$ m s^{-1}; $Q_o = 0.0138$ m^3 s^{-1}; $M_o = 0.0242$ m^4 s^{-2}; $\Delta x = 12D$). Tabulated velocities are a comparison of the computed velocity magnitude obtained by Taylor's solution, and by the distributed point sink approach (mean deviation = 0.60 %).

viscosity (which is valid to first order). More often, boundary layer approximations have been used for the jet flow, resulting in integral jet models that solve for the characteristic jet properties; on the other hand, the flow outside of the jet can be treated as irrotational by using the inviscid approximation (Taylor 1958).

As far as the outside irrotational flow is concerned, the jet acts as a distributed entrainment sink. Taylor's concept is attractive as it lends itself readily to general application (Lai 2009). Suppose the buoyant jet trajectory and the entrainment flow of every 'jet element' can be predicted. Then the outside entrainment flow induced at a given point (x_p, y_p, z_p) due to one jet can be predicted as the sum of the velocities induced by the point sinks (with known strength) in all the jet elements. Also, the induced velocity due to all the jets can be similarly summed (equations (2.3) and (2.4)). Bottom and free surface boundaries can be accounted for using the method of images.

If this concept is applied to a simple jet (Lai 2009), the induced entrainment velocity field in the plane of symmetry agrees well with Taylor's analytical solution, which shows a set of confocal parabolas with curvature decreasing downstream, even at a coarse discretization ($\Delta x = 0.02H = 12D$) of the jet element (figure 21). The velocity magnitudes predicted by the two approaches are also in excellent agreement.

The concept can readily be extended to predict multiple jet-induced external flow. The predicted flow can be compared with a 3D solution of the RANS equations in Cartesian coordinates using the FLUENT software ($D = 0.01$ m and $u_o = 1$ m s^{-1})

https://doi.org/10.1017/jfm.2012.332 Published online by Cambridge University Press

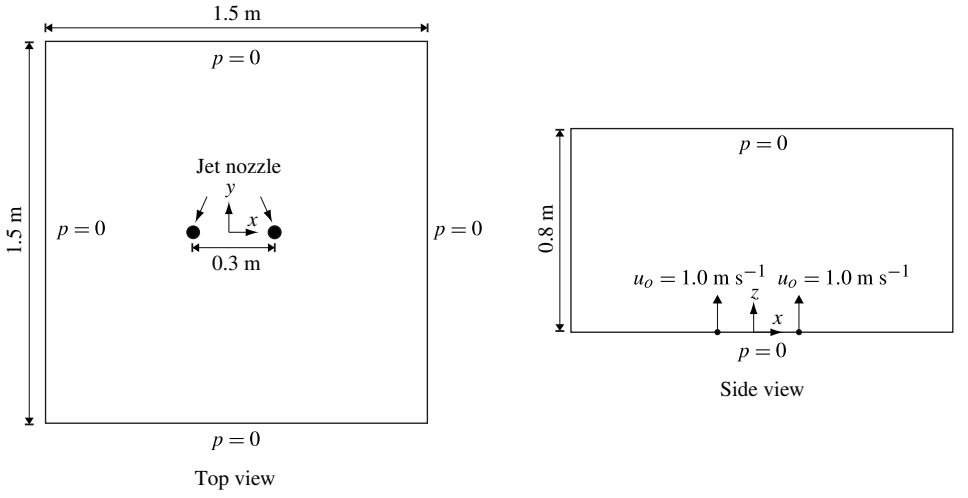


FIGURE 22. Computational domain of the 3D RANS numerical computation for twin jet-induced flow ($D = 0.01$ m; u_o = initial jet velocity).

using a realizable k–ϵ model (Shih *et al.* 1995) for turbulent closure. The jet nozzle area is resolved by 218 cells; a total of 479 200 cells are used (Lai 2009). The zero-pressure boundary condition is used in all six faces of the domain (figure 22). It is found that the external flow agrees with the CFD solution for both single and widely separated twin jets. Figure 23 shows the comparison of predicted velocities with the FLUENT solution in the plane of symmetry (vertical and lateral velocity) for two widely separated jets. It should be noted that in general the numerical solution has its own limitations: the external flow depends somewhat on the boundary conditions imposed; the predicted jet spreading rate may depend greatly on the turbulence model approximations (e.g. see discussion by Craft & Launder (2001) on wall jets); and there are intrinsic difficulties in the modelling of the scalar field (a constant turbulent Schmidt number). However, as the overall jet flow and jet spreading rate are well predicted ($\mathrm{d}b_g/\mathrm{d}s = 0.115$ versus the experimental value of 0.114), the CFD solution can serve as a useful reference.

Appendix B. Computation of jet group velocity field by superposition method

For an axisymmetric pure jet discharge (in z direction), the governing momentum equation can be written in terms of the time-mean normal and shear stresses:

$$\frac{\partial(r\overline{U^2})}{\partial z} + \frac{1}{r}\frac{\partial(r\overline{UV})}{\partial r} = 0, \tag{B 1}$$

where U and V are instantaneous velocities. Reichardt's inductive hypothesis for turbulent closure assumes that the lateral gradient of the shear stress is proportional to the transverse gradient of the z momentum (Hinze 1975):

$$\overline{UV} = -\Lambda(z)\frac{\partial \overline{U^2}}{\partial r}, \tag{B 2}$$

where $\Lambda(z) = (b/2)(\mathrm{d}b/\mathrm{d}z)$ and $b(z)$ is a characteristic jet width that is a function only of z.

https://doi.org/10.1017/jfm.2012.332 Published online by Cambridge University Press

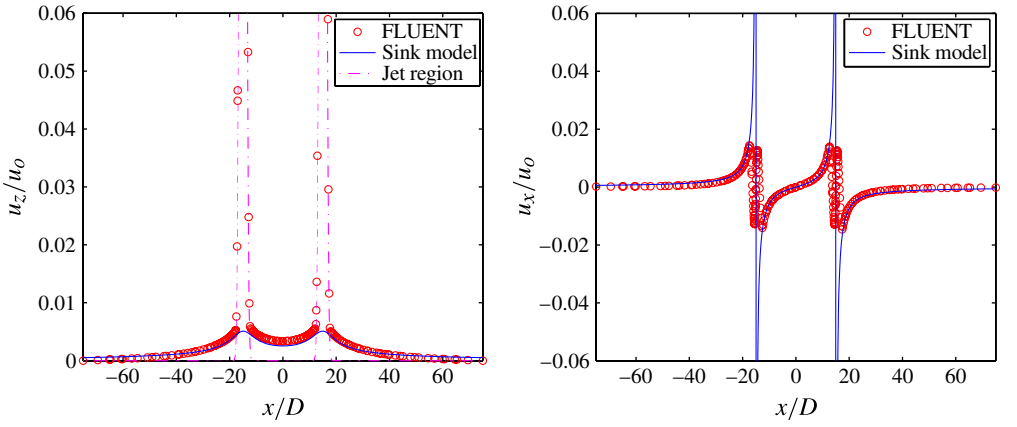


FIGURE 23. (Colour online) Comparison between model predictions and FLUENT computations for twin jet discharges at $z = 10D$ ($D = 0.01$ m; $u_o = 1$ m s^{-1}; nozzle spacing $s = 30D$).

Substituting (B 2) into (B 1) and neglecting turbulent contributions to the mean jet momentum flux results in an equation linear in $u^2 = \overline{U^2}$ where u is the time-mean z velocity:

$$\frac{\partial u^2}{\partial z} - \Lambda \left\{ \frac{\partial^2 u^2}{\partial r^2} + \frac{1}{r}\frac{\partial u^2}{\partial r} \right\} = 0. \tag{B 3}$$

The linearity of the equation in jet momentum permits the method of superposition to be used in multiple axisymmetric jet discharges.

Alternatively, the superposition approach can be shown to be valid by considering conservation of momentum. Consider N vertical jets, each with initial momentum flux M_o, discharging into an otherwise stagnant fluid in the $+z$ direction. By momentum flux conservation, at a given level z the jet group momentum flux M_{N_J} is equal to the sum of the momentum flux of N non-interacting individual jets (i.e. each jet being considered as a single free jet):

$$M_{N_J} = \int u_{N_J}^2(x, y, z)\, \mathrm{d}A = M_1 + M_2 + \cdots + M_N = NM_o, \tag{B 4}$$

where the area integral is taken over the xy plane. Then

$$\int u_{N_J}^2(x, y, z)\, \mathrm{d}A = \int u_1^2\, \mathrm{d}A + \int u_2^2\, \mathrm{d}A + \cdots + \int u_N^2\, \mathrm{d}A, \tag{B 5}$$

where $u_i(x, y, z)$ is the velocity field induced by the ith independent jet, and $u_{N_J}(x, y, z)$ is the velocity field of the jet group. It can be seen that a solution to (B 5) is

$$u_{N_J}^2(x, y, z) = u_1^2 + u_2^2 + \cdots + u_N^2. \tag{B 6}$$

In other words, at each point of a given level z, the momentum induced by the individual jets can be superimposed to give the momentum (and thus velocity field) of the jet group.

https://doi.org/10.1017/jfm.2012.332 Published online by Cambridge University Press

Appendix C. Computation of plume group velocity field by superposition method

The superposition approach can be extended to compute the velocity field of a plume group. For multiple plumes it was suggested that the velocity field can be obtained by superposition of the kinetic energy flux $\sim \int u^3 \, \mathrm{d}A$. The hypothesis can be justified heuristically as below, to be validated by CFD calculations. It is useful to consider first the mechanical energy conservation equation of a round buoyant jet in cylindrical coordinates (z, r), where z is the vertical and r is the radial coordinate:

$$\frac{\partial u^3}{\partial z} + \frac{1}{r}\frac{\partial r u^2 v}{\partial r} = 2ug' - \frac{2u}{r}\frac{\partial (r\overline{u'v'})}{\partial r}. \tag{C 1}$$

Here $u(z, r)$ and $v(z, r)$ are the turbulent-mean z and r velocity, respectively, g' is the local reduced gravity, and u' and v' are the turbulent velocity fluctuations in the z and r direction, respectively. Equation (C 1) can be obtained from the governing continuity and momentum equations. The dependence of the entrainment coefficient α on the local jet densimetric Froude number Fr_L, $\alpha = \alpha_j + (\alpha_p - \alpha_j)\,(Fr_p/Fr_L)^2$ (Priestley & Ball 1955), can then be derived from the integral form of the continuity, momentum and kinetic energy equations. Specifically, it can be shown that the integral form of (C 1) can be written as (Fox 1970; Lee & Jirka 1981; Lai & Lee 2012)

$$\frac{\partial}{\partial z}\int u^3 \, \mathrm{d}A = \frac{2\pi\lambda^2}{1+\lambda^2} u_m g'_m b_g^2 - \frac{2}{3}\pi u_m^3 \alpha_j b_g, \tag{C 2}$$

where u_m and g'_m are the velocity and reduced gravity at the centreline of the buoyant jet, respectively, and b_g is the Gaussian jet half-width. In the above, α_j and α_p are the entrainment coefficients of a momentum jet and plume, respectively, and $Fr_L = u_m/\sqrt{g'_m b_g}$ is the local jet densimetric Froude number. It can be shown that $\alpha \to \alpha_j$ for momentum jets, that $g'_m \to 0$, and that all buoyant jets tend to be plumes far away from the source, with $Fr_L \to Fr_p$, which is the asymptotic plume densimetric Froude number, $\alpha \to \alpha_p$. For a round plume, $Fr_p = \sqrt{5\lambda^2/4\alpha_p} = 4.6$ for $\alpha = 0.085$ and $\lambda = 1.2$. (A recent summary of α and λ can be found in Kaminski, Tait & Carazzo (2005).)

Adopting the classical solution of $u_m = 4.71 F_o^{1/3} z^{-1/3}$ and $b_g = 0.105z$ for a pure plume (Rouse, Yih & Humphreys 1952), and assuming Gaussian velocity and buoyancy profiles, we have

$$\frac{2\pi\lambda^2}{1+\lambda^2} u_m g'_m b_g^2 = 2F, \tag{C 3}$$

and adopting $\alpha_j = 0.057$ we obtain

$$\tfrac{2}{3}\pi u_m^3 \alpha_j b_g \approx 1.3F, \tag{C 4}$$

where F is the plume buoyancy flux, which is conserved.

From (C 2) the plume kinetic energy flux can thus be related to the buoyancy flux as

$$\frac{\partial E}{\partial z} \sim \frac{\partial}{\partial z}\int u^3 \, \mathrm{d}A \approx 0.7F, \tag{C 5}$$

and thus

$$\int u^3 \, \mathrm{d}A \approx kFz \tag{C 6}$$

https://doi.org/10.1017/jfm.2012.332 Published online by Cambridge University Press

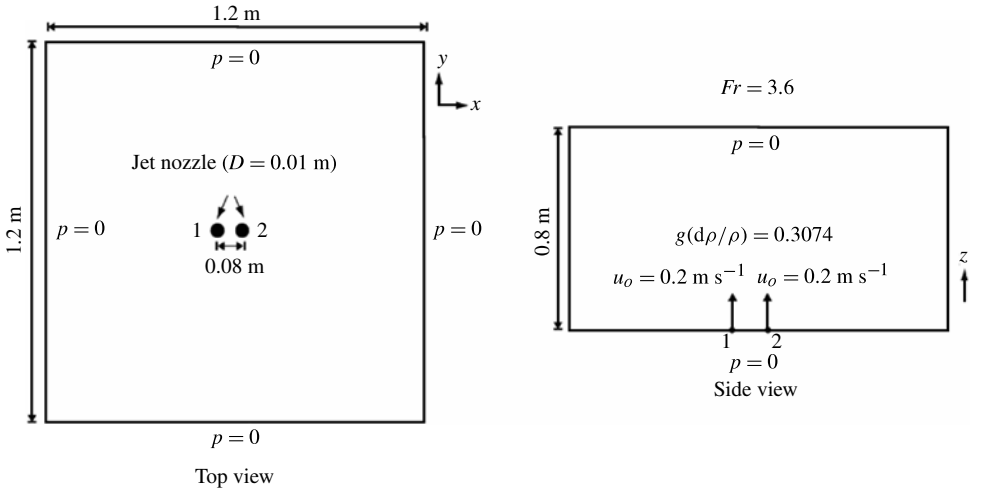


FIGURE 24. Computational domain and boundary conditions in the 3D RANS numerical computation for twin plume-induced flow ($D = 0.01$ m, $Fr = 3.6$).

in a plume, where $k \approx 0.7$. Now by the conservation of buoyancy flux, at a given level z, the plume group buoyancy flux F_{N_J} is equal to the sum of the buoyancy flux of the N non-interacting individual plumes:

$$F_{N_J} = F_1 + F_2 + \cdots + F_N, \tag{C 7}$$

$$kF_{N_J} z = kF_1 z + kF_2 z + \cdots + kF_N z. \tag{C 8}$$

Assuming that the kinetic energy flux of a plume group can be expressed in terms of the buoyancy flux in the same way as a single plume, we have

$$\int u_{N_J}^3(x, y, z)\,\mathrm{d}A = \int u_1^3\,\mathrm{d}A + \int u_2^3\,\mathrm{d}A + \cdots + \int u_N^3\,\mathrm{d}A. \tag{C 9}$$

A solution to (C 9) is

$$u_{N_J}^3(x, y, z) = u_1^3 + u_2^3 + \cdots + u_N^3. \tag{C 10}$$

The above shows heuristically that the local kinetic energy at each point of a given level z of individual plumes can be superimposed to give the kinetic energy (and thus velocity field) of the plume group. This hypothesis can be further tested by detailed 3D numerical solution of the RANS equations.

C.1. *A computational study of kinetic energy superposition*

We have further carried out a computational study using FLUENT to ensure the validity of kinetic energy superposition for a plume group. Twin round plumes discharging into stagnant fluid, each with nozzle diameter $D = 0.01$ m, were considered. Other discharge parameters are: $s = 0.08$ m, $u_o = 0.2$ m s^{-1}, $(\Delta\rho/\rho)g = 0.3074$ and $Fr = 3.6$. The discharge parameters, physical domain and boundary conditions are given in figure 24.

Three runs were performed, keeping the discharge parameters for each individual plume unchanged: (i) discharge with both plumes; (ii) discharge with plume 1 blocked (by setting the nozzle as a zero-pressure boundary); and (iii) discharge with plume 2

https://doi.org/10.1017/jfm.2012.332 Published online by Cambridge University Press

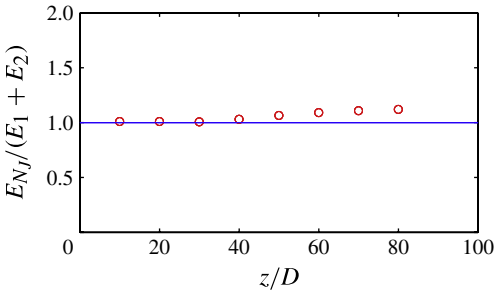


FIGURE 25. (Colour online) The ratio of kinetic energy (KE) flux of twin plume discharge to the sum of the KE fluxes of individual plumes along z.

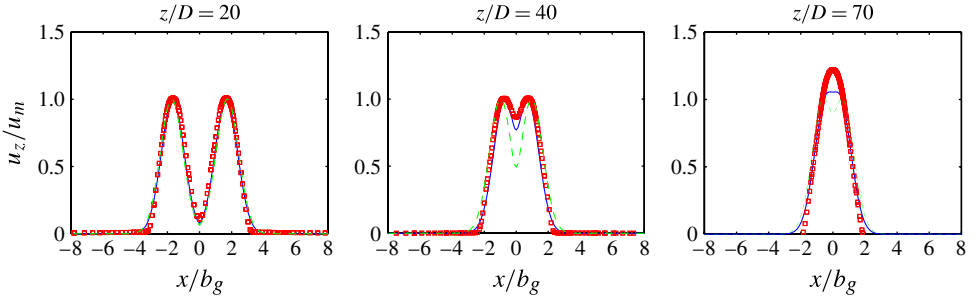


FIGURE 26. (Colour online) Comparison of the computed twin plume velocity profile and the prediction using superposition of kinetic energy along z: solid line, prediction; dashed line, straight plume superposition; symbols, FLUENT simulation. Here b_g is the computed Gaussian jet width of a single plume.

blocked. In the computations, the convergence criterion was based on previous calculations of buoyant jet discharges (Kuang *et al.* 2006).

The computed kinetic energy flux E is obtained by summing up $(u^3\,\mathrm{d}A)/2$ at every computational grid point at a given z, where $\mathrm{d}A$ is the cross-sectional grid area at z. Figure 25 shows that the kinetic energy flux of twin plume discharges (E_{N_J}) is close to that obtained by summing the kinetic energy flux of each individual plume (E_1 and E_2) along z. This supports $\int u_{N_J}^3\,\mathrm{d}A = \int u_1^3\,\mathrm{d}A + \int u_2^3\,\mathrm{d}A$ and thus the validity of the kinetic energy superposition $u_{N_J}^3 = u_1^3 + u_2^3$. The numerical solution also demonstrates that $E \approx kFz$ ($k \approx 0.7$) for both the individual plume and the plume group (not shown).

Finally, the computed velocity profile of the twin plume discharge along z is shown in figure 26. The prediction of velocity profile can be made by superposition of u^3 of plume 1 and plume 2. As indicated by the dashed line, accounting only for the plume interaction due to their overlapping (i.e. superposition of u^3 for straight plumes without deflection) gives unsatisfactory predictions – the merging height is over-predicted. Satisfactory predictions can however be obtained by accounting for the plume deflection (the plume deflected trajectory is obtained by searching the local maximum of plume velocity profile until the two plumes merge). As previously discussed, the FLUENT computation serves mainly as a reference as the CFD solution based on two-equation k–ϵ modelling has its own limitations.

https://doi.org/10.1017/jfm.2012.332 Published online by Cambridge University Press

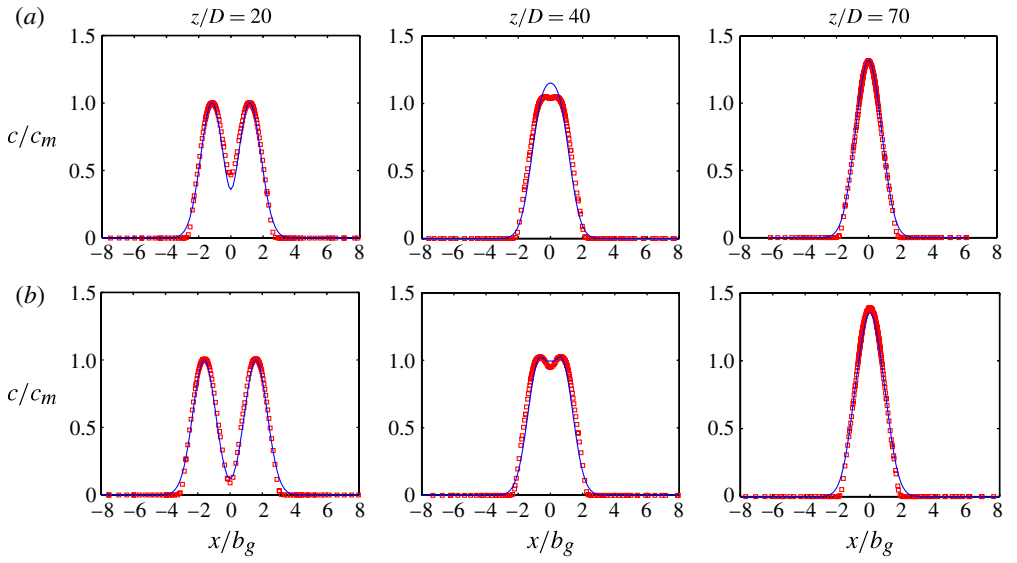


FIGURE 27. (Colour online) Comparison of the computed concentration profile and the prediction using the superposition approach, for (*a*) twin jets and (*b*) twin plumes: solid line, prediction; symbols, FLUENT simulation. Here b_g is the computed Gaussian jet width of a single jet/plume.

Appendix D. Computation of jet and plume group concentration field by superposition method: comparison with CFD solution

Reichardt's hypothesis was extended to compute the concentration field by Hodgson *et al.* (1999) of a jet group. Alternatively, by tracer mass conservation and using a similar argument as in appendices B and C, it can be shown that uc at each point of a given level z can be superimposed to give the concentration field $c_{N_J}(x, y, z)$ of the jet or plume group after $u_{N_J}(x, y, z)$ is computed (using appendix B for jets and appendix C for plumes). Mathematically,

$$u_{N_J} c_{N_J} = u_1 c_1 + u_2 c_2 + \cdots + u_N c_N, \tag{D 1}$$

$$c_{N_J} = \frac{u_1 c_1 + u_2 c_2 + \cdots + u_N c_N}{u_{N_J}}. \tag{D 2}$$

The prediction of concentration profile by the superposition method accounting for dynamic interaction is compared with the 3D CFD numerical solution. The discharge configuration of the twin jets and plumes are the same as that in appendix C, with the buoyancy effect turned off for the jet simulation (fluid density is set as constant). Figure 27(*a*,*b*) show the comparison of the prediction by the superposition approach and the CFD simulation of twin jets and plumes, respectively. The agreement is in general good. Similar levels of agreement are also seen in other cross-sections.

Appendix E. Asymptotic behaviour of superposition solutions

Two further examples are given to show the validity of the superposition approach. We first consider a single row of 51 vertical jets, each with jet nozzle diameter $D = 0.01$ m and initial velocity $u_o = 1.0$ m s^{-1}, discharging into stagnant fluid. The centre-to-centre distance s of the jet group is $7D$. The objective is to compute the jet group centreline velocity and concentration, which is expected to be equal to that of a

https://doi.org/10.1017/jfm.2012.332 Published online by Cambridge University Press

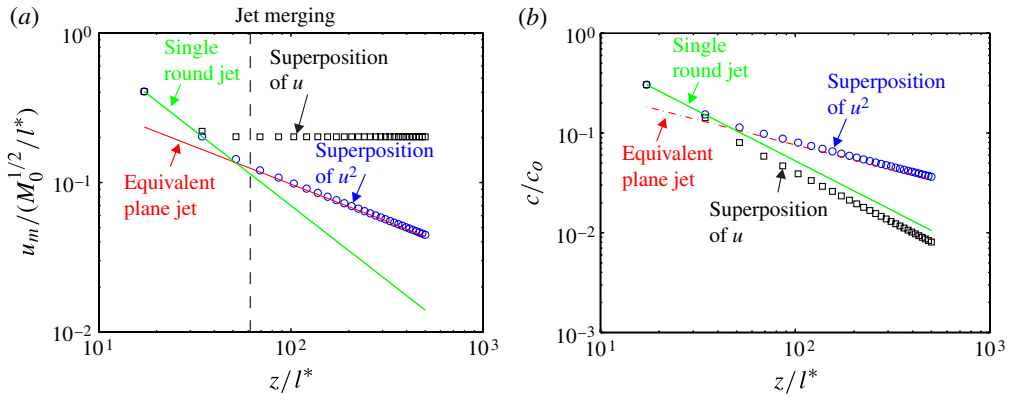


FIGURE 28. (Colour online) Predicted (*a*) centreline velocity of a jet group and (*b*) centreline concentration of a jet group using the superposition approach. $l^* = D$ for a round jet, and $l^* = \sqrt{4b_s s/\pi}$ for an equivalent slot jet, where b_s is the slot width.

single free jet initially, and gradually converges to that of an equivalent slot jet (after full jet merging) with the same total volume, momentum flux and tracer mass flux as the jet group.

Figure 28(*a*) shows the predicted centreline velocity of the jet group. The centreline velocity follows that of a single free jet initially, and after jet merging it converges to that of an equivalent plane jet (see e.g. Wood *et al.* (1993) for a summary of single round and plane jet/plume properties). Figure 28(*b*) shows that, with the correct jet group velocity computed, the concentration field of a jet group can be predicted by superimposing uc. Also shown in both figures are the predictions if the jet velocity is superimposed (e.g. Davidson, Papps & Wood 1994) – which appear to give noticeably poorer predictions.

The second example illustrates the superposition of kinetic energy for a plume group. We consider 51 vertical plumes, each with nozzle diameter $D = 0.01$ m and initial velocity $u_o = 0.01$ m s^{-1}, discharging into stagnant fluid. The centre-to-centre distance s of the jet group is $7D$. The relative density difference is $\Delta\rho/\rho = 0.001$, giving the plume densimetric Froude number $Fr \approx 1.0$.

Figure 29(*a*,*b*) shows the predicted centreline velocity and concentration of the plume group. By superimposing u^3, both the predicted velocity and concentration follow the expected trend of a plume group: initially the plume centreline velocity and concentration follow that of a single free plume; after plume merging they follow that of an equivalent plane plume with a constant centreline velocity. However, if either u^2 or u are superimposed instead, the centreline velocity of the plume group can be seen to be significantly over-predicted (figure 29*a*). Correspondingly, the plume group centreline concentration is seen to be significantly under-predicted (figure 29*b*).

Appendix F. Sensitivity of predicted multiple jet trajectories to control volume definition

As an exact momentum balance is performed, the calculations for the multiple jet trajectories are not dependent on the choice of the control volume – provided the velocities (momentum flux) and pressure force can be accurately determined on the control surface boundaries. In practice, the boundaries of the control volume or computational box should be defined in the flow external to the jet (e.g. a suitable

https://doi.org/10.1017/jfm.2012.332 Published online by Cambridge University Press

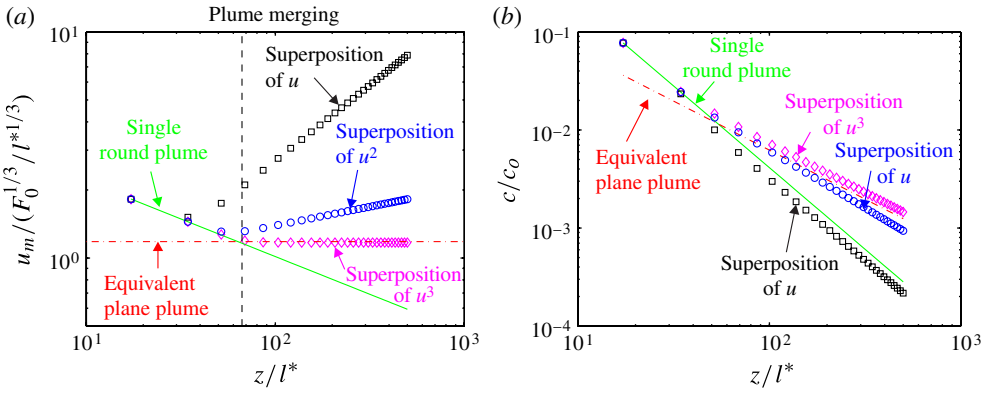


FIGURE 29. (Colour online) Predicted (*a*) centreline velocity of a plume group and (*b*) centreline concentration of a plume group using the superposition approach. $l^* = D$ for a round jet, and $l^* = \sqrt{4b_s s/\pi}$ for an equivalent slot jet, where b_s is the slot width.

z/D	x/D for no-flux boundary	x/D for circle with radius B	x/D for circle with radius $\sqrt{2}B$
0	0	0	0
10	11.0292	11.0161	11.0306
20	12.6215	12.7933	12.8119
30	13.0251	13.3439	13.3555
40	12.8529	13.2614	13.2575
50	12.3070	12.7393	12.7106
60	11.4734	11.8532	11.7838
70	10.3923	10.6273	10.4090
80	9.0821	9.0393	9.1018

TABLE 1. Tabulated trajectory of a rosette buoyant jet group ($N_J = 6$) in stagnant fluid with alternative control volume definitions (cf. figures 19(*a*) and 30).

symmetry plane on which normal velocities are zero, or a small circle with boundaries just enclosing and outside the turbulent buoyant jet). The computation of multiple jet trajectories by the dynamic interaction model is not sensitive to the exact choice of a control volume with boundaries appropriately defined in the external irrotational flow. As a sensitivity study, we consider a rosette jet group discharge ($N_J = 6$). The jet group parameters are $D = 0.0044$ m, $\Delta\rho/\rho_a = 0.1266$ and $u_o = 0.365$ m s^{-1}. As shown in figure 19(*a*), three control volume definitions can be adopted: (i) a pie-shaped control volume, with two lateral radial no-flux boundaries; (ii) a local control volume, i.e. a circle just enclosing the jet with radius defined by the local top-hat jet half-width, $r = B$; and (iii) the same local control volume with a larger radius, $r = \sqrt{2}B$.

Figure 30 shows the comparison of the predicted trajectories obtained by adopting the three different control volume definitions. The difference is graphically indistinguishable; the maximum difference in predicted x position is 0.4, 3.2 and 1.6 % for $z/D = 20$, 40 and 80, respectively (table 1). Similar results are obtained for the computation of a rosette jet group in a weak cross-flow, $K = 12.2$ (figure 31).

https://doi.org/10.1017/jfm.2012.332 Published online by Cambridge University Press

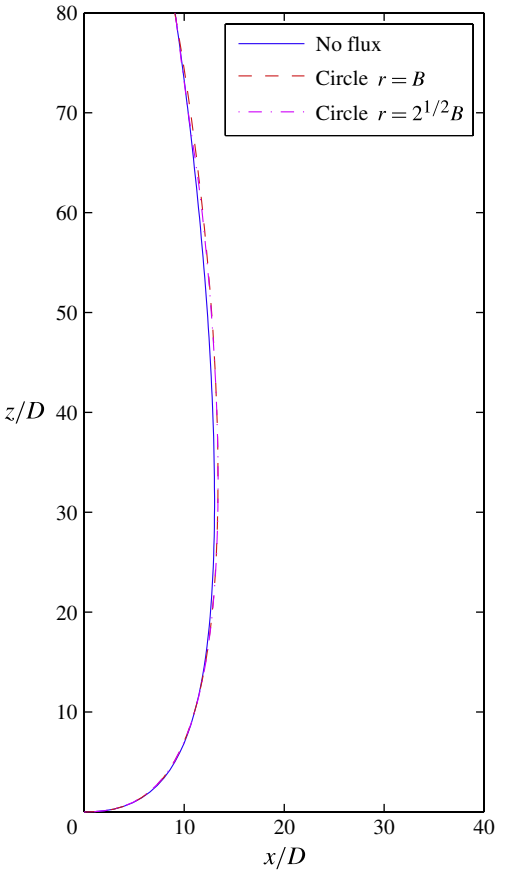


FIGURE 30. (Colour online) The predicted rosette buoyant jet group trajectory using alternative control volume definitions ($N_J = 6$; cf. figure 12*b*).

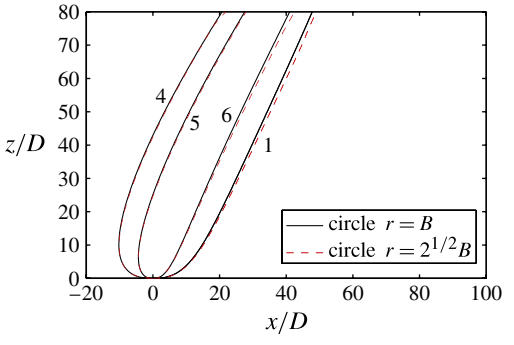


FIGURE 31. (Colour online) The predicted rosette buoyant jet group trajectory in a cross-flow using alternative control volume definitions ($K = 12.2$; cf. figures 19*b* and 20*a*).

REFERENCES

BAINES, W. D. & KEFFER, K. F. 1974 Entrainment by a multiple source turbulent jet. *Adv. Geophys.* **18B**, 289–298.

BATCHELOR, G. K. 1967 *An Introduction to Fluid Dynamics*. Cambridge University Press.

https://doi.org/10.1017/jfm.2012.332 Published online by Cambridge University Press

CRAFT, T. J. & LAUNDER, B. E. 2001 On the spreading mechanism of the three-dimensional turbulent wall jet. *J. Fluid Mech.* **435**, 305–326.

DAVIDSON, M. J. 1989 The behaviour of single and multiple horizontally discharged buoyant jets in a non-turbulent ambient fluid. PhD thesis, University of Canterbury, New Zealand.

DAVIDSON, M. J., GASKIN, S. & WOOD, I. R. 2002 A study of a buoyant axisymmetric jet in a small co-flow. *J. Hydraul. Res.* **40** (4), 477–489.

DAVIDSON, M. J., PAPPS, D. A. & WOOD, I. R. 1994 The behaviour of merging buoyant jets. In *Recent Research Advances in the Fluid Mechanics of Turbulent Jets and Plumes* (ed. P. A. Davies & M. J. Valente Neves), pp. 465–478. Dordrecht.

FISCHER, H. B., LIST, E. J., KOH, R. C. Y., IMBERGER, J. & BROOKS, N. H. 1979 *Mixing in Inland and Coastal Waters*. Academic Press.

FOX, D. G. 1970 Forced plume in a stably stratified fluid. *J. Geophys. Res.* **75**, 6818–6835.

GASKIN, S. J. 1995 Single buoyant jet in a crossflow and the advected line thermal. PhD thesis, University of Canterbury, New Zealand.

HINZE, J. O. 1975 *Turbulence*. McGraw-Hill.

HODGSON, J. E., MOAWAD, A. K. & RAJARATNAM, N. 1999 Concentration field of multiple circular turbulent jets. *J. Hydraul. Res.* **37** (2), 249–256.

KAMINSKI, E., TAIT, S. & CARAZZO, G. 2005 Turbulent entrainment in jets with arbitrary buoyancy. *J. Fluid Mech.* **526**, 361–376.

KAYE, N. B. & LINDEN, P. F. 2004 Coalescing axisymmetric turbulent plumes. *J. Fluid Mech.* **502**, 41–63.

KNYSTAUTAS, R. 1964 The turbulent jet from a series of holes in line. *Aeronaut. Q.* **15**, 1–28.

KUANG, C. P., LEE, J. H. W., LIU, S. G. & GU, J. 2006 Numerical study on plume interaction above an alternating diffuser in stagnant water. *China Ocean Engng* **20** (2), 289–302.

KWON, S. J. 2005 Behavior of buoyant discharges from a rosette-type diffuser. PhD thesis, Seoul National University.

LAI, A. C. H. 2009 Mixing of a rosette buoyant jet group. PhD thesis, The University of Hong Kong.

LAI, A. C. H. & LEE, J. H. W. 2010 Multiple tandem jet interaction in a crossflow. *J. Hydrodyn.* B **22** (5/suppl. 1), 639–643.

LAI, C. K. C. & LEE, J. H. W. 2012 Mixing of inclined dense jets in stationary ambient. *J. Hydro-environ. Res.* **6** (1), 9–28.

LAI, A. C. H., YU, D. & LEE, J. H. W. 2011 Mixing of a rosette jet group in a crossflow. *J. Hydraul. Engng ASCE* **137** (8), 787–803.

LAMB, H. 1932 *Hydrodynamics*, 6th edn. Dover.

LEE, J. H. W. & CHU, V. H. 2003 *Turbulent Jets and Plumes – a Lagrangian Approach*. Kluwer.

LEE, A. W. T. & LEE, J. H. W. 1998 Effect of lateral confinement on initial dilution of vertical round buoyant jet. *J. Hydraul. Engng ASCE* **124** (3), 263–279.

LEE, J. H. W. & GREENBERG, M. D. 1984 Line momentum source in shallow inviscid fluid. *J. Fluid Mech.* **145**, 287–304.

LEE, J. H. W. & JIRKA, G. H. 1980 Multiport diffuser as line source of momentum in shallow water. *Water Resour. Res.* **16** (4), 695–708.

LEE, J. H. W. & JIRKA, G. H. 1981 Vertical round buoyant jet in shallow water. *J. Hydraul. Div. ASCE* **107** (HY12), 1651–1675.

LINDEN, P. F. 1999 The fluid mechanics of natural ventilation. *Annu. Rev. Fluid Mech.* **31**, 201–238.

LISETH, P. 1970 Mixing of merging buoyant jets from a manifold in stagnant receiving water of uniform density. PhD thesis, University of California.

LISETH, P. 1976 Wastewater disposal by submerged manifolds. *J. Hydraul. Div. ASCE* **102** (1), 1–14.

MARSTERS, G. F. 1977 Interaction of two plane, parallel jets. *AIAA J.* **15** (12), 1756–1762.

MILLER, D. R. & COMINGS, E. W. 1960 Force–momentum fields in a dual jet flow. *J. Fluid Mech.* **7**, 237–256.

MILNE-THOMSON, L. M. 1968 *Theoretical Hydrodynamics*. Macmillan.

https://doi.org/10.1017/jfm.2012.332 Published online by Cambridge University Press

MONISMITH, S. G., KOSEFF, J. R., THOMPSON, J. K., O'RIORDAN, C. A. & NEPF, H. M. 1990 A study of model bivalve siphon currents. *Limnol. Oceanogr.* **35** (3), 680–696.

MORTON, B. R., TAYLOR, G. I. & TURNER, J. S. 1956 Turbulent gravitational convection from maintained and instantaneous sources. *Proc. R. Soc. Lond.* A **234**, 1–23.

PANI, B. S. & DASH, R. 1983 Three-dimensional single and multiple free jets. *J. Hydraul. Engng ASCE* **109** (2), 254–269.

PANI, B. S., LAI, A. C. H. & LEE, J. H. W. 2009 Application of Reichardt's hypothesis for multiple coflowing jets. *J. Hydro-environ. Res.* **3** (3), 121–128.

PERA, L. & GEBHART, B. 1975 Laminar plume interactions. *J. Fluid Mech.* **68**, 259–271.

PRATTE, B. D. & KEFFER, J. F. 1972 The swirling turbulent jet. *Trans. ASME: J. Basic Engrg* **94** (4), 739–748.

PRIESTLEY, C. H. B. & BALL, F. K. 1955 Continuous convection from an isolated source of heat. *Q. J. R. Meteorol. Soc.* **81** (348), 144–157.

ROBERTS, P. J. W. & SNYDER, W. H. 1993*a* Hydraulic model study for Boston outfall I. Riser configuration. *J. Hydraul. Engng ASCE* **119** (9), 970–987.

ROBERTS, P. J. W. & SNYDER, W. H. 1993*b* Hydraulic model study for Boston outfall II. Environmental performance. *J. Hydraul. Engng ASCE* **119** (9), 988–1002.

ROUSE, H., YIH, C. S. & HUMPHREYS, H. W. 1952 Gravitational convection from a boundary source. *Tellus* **4**, 201–210.

SEO, I. W., KWON, S. J. & YEO, H. K. 2004 Merging characteristics of buoyant discharges from rosette-type diffusers in shallow water. *J. Civil Engng KSCE* **8** (6), 679–688.

SHIH, T. H., LIOU, W. W., SHABBIR, A., YANG, Y. & ZHU, J. 1995 A new k–ϵ eddy viscosity model for high Reynolds number turbulent flows. *Comput. Fluids* **24** (3), 227–238.

SORRELL, F. Y. & SMITH, B. W. 1982 Discharge jet interaction with multiple port diffusers. *J. Fluids Engng* **104**, 40–45.

SQUIRE, H. B. 1951 The round laminar jet. *Q. J. Mech. Appl. Maths* **4**, 321–329.

TAYLOR, G. I. 1958 Flow induced by jets. *J. Aerosp. Sci.* **25**, 464–465.

TURNER, J. S. 1986 Turbulent entrainment: the development of the entrainment assumption, and its application to geophysical flows. *J. Fluid Mech.* **173**, 431–471.

WOOD, I. R., BELL, R. G. & WILKINSON, D. L. 1993 *Ocean Disposal of Wastewater*. World Scientific.

YANNOPOULOS, P. C. & NOUTSOPOULOS, G. C. 2006 Interaction of vertical round turbulent buoyant jets. Part II: superposition method. *J. Hydraul. Res.* **44** (2), 233–248.

https://doi.org/10.1017/jfm.2012.332 Published online by Cambridge University Press